Global and Planetary Change 253 (2025) 104972

Contents lists available at ScienceDirect

Global and Planetary Change

journal homepage: www.elsevier.com/locate/gloplacha

Research Article

Spatio-temporal changes in interannual sea level along the world coastlines

Lancelot Leclercq [a], Habib B. Dieng [b], Anny Cazenave [a,*], Florence Birol [a], Julius Oelsmann [c], Marcello Passaro [d], Svetlana Jevrejeva [e], Erwin Bergsma [f], Sarah Connors [g]

[a] Université de Toulouse, LEGOS (CNES/CNRS/IRD/UT3), 31401 Toulouse, Cedex 9, France
[b] Université Assane Seck de Ziguinchor, Diabir-Ziguinchor, BP 523, 27000 Ziguinchor, Senegal
[c] Tulane University, School of Science & Engineering, 101 Lindy Boggs Center, New Orleans, LA 70118, USA
[d] Technical University of Munich, Munich 80333, Germany
[e] National Oceanography Center, L3 5DA Liverpool, UK
[f] Centre National d'Etudes Spatiales, 31401 Toulouse, Cedex 9, France
[g] European Space Agency, Climate Office, Oxfordshire OX11 0F, UK

ARTICLE INFO

Editor: Dr. Alan Haywood

Keywords:
Coastal sea level changes
Interannual sea level changes
Internal climate modes

ABSTRACT

To investigate how coastal sea level evolves at interannual time scales from one region to another, we perform an Empirical Orthogonal Function (EOF) decomposition of coastal sea level time series derived from reprocessed coastal altimetry data over a 20-year long time span (2002−2021), at 1132 virtual coastal stations homogeneously distributed along the world coastlines. This analysis is first performed globally and then over selected coastal regions. Consistent with previous studies, the results show the dominant influence of internal climate modes, in particular ENSO (El Niño Southern Oscillation), on the interannual coastal sea level variability. But our study also reports novel findings in coastal sea level: (1) a regime shift between 2008 and 2012, with increased sea level rate after that date in many coastal regions, and (2) a 6-year cycle, notably along the northeast and northwest coasts of America (north of 40°N) and along the Indian coast of Indonesia. Additional EOF analyses are done using both gridded altimetry sea level data from the Copernicus Climate Change Service and an ensemble mean of four ocean reanalyses, in three successive coastal bands: 0-50 km, 50-100 km and 100-500 km from land. They confirm the strong influence of internal climate modes at the coast but also show that results in the cross-shore direction towards the open ocean are similar to those at the coast. This study based on three different datasets shows that the strong influence of internal climate modes on sea level interannual variability in the world coastal zones is not limited to the open ocean but also dominates sea level changes very close to the coast. It also shows evidence of a regime shift in the rate of change of coastal sea level between 2008 and 2012 and the presence of a 6-year oscillation in coastal sea level, possibly linked to the recent discovery of a 6-year cycle in the whole climate system.

1. Introduction

Sea level varies over a broad range of spatio-temporal scales. The global mean sea level (GMSL) has not only risen at a mean rate of 3.5 ±− 0.3 mm/yr since the beginning of the high- precision altimetry era (i.e., since the early 1990s) but has also accelerated by 0.12 ± 0.05 mm/yr^2 (e.g., Guérou et al., 2023; Hamlington et al., 2024). The GMSL rise and acceleration mostly result from ocean warming and land ice melt, a consequence of anthropogenic global warming (IPCC, 2019, 2022). Acceleration in global mean sea surface temperature driven by Earth's energy imbalance has also been recently reported (Merchant et al., 2025).

At regional scale, spatial trend patterns superimpose the global mean rise (Fig. 1). These are large-scale features mostly due to non-uniform ocean heat content change in response to ocean circulation changes caused by different forcing factors (e.g., wind stress or direct heat and mass exchanges between the atmosphere and the ocean) (Stammer et al., 2013; Hamlington et al., 2020; Cazenave and Moreira, 2022). In some oceanic areas, salinity changes also play a role. These large-scale spatial patterns are still largely driven by natural (internal) climate modes (e.g., Palanisamy et al., 2015; Han et al., 2017) although in some regions, anthropogenic forcing is now emerging (e.g., Fasullo et al., 2020).

* Corresponding author.
E-mail address: anny.cazenave@univ-tlse3.fr (A. Cazenave).

https://doi.org/10.1016/j.gloplacha.2025.104972
Received 10 February 2025; Received in revised form 15 May 2025; Accepted 3 July 2025
Available online 4 July 2025
0921-8181/© 2025 The Authors. Published by Elsevier B.V. This is an open access article under the CC BY license (http://creativecommons.org/licenses/by/4.0/).

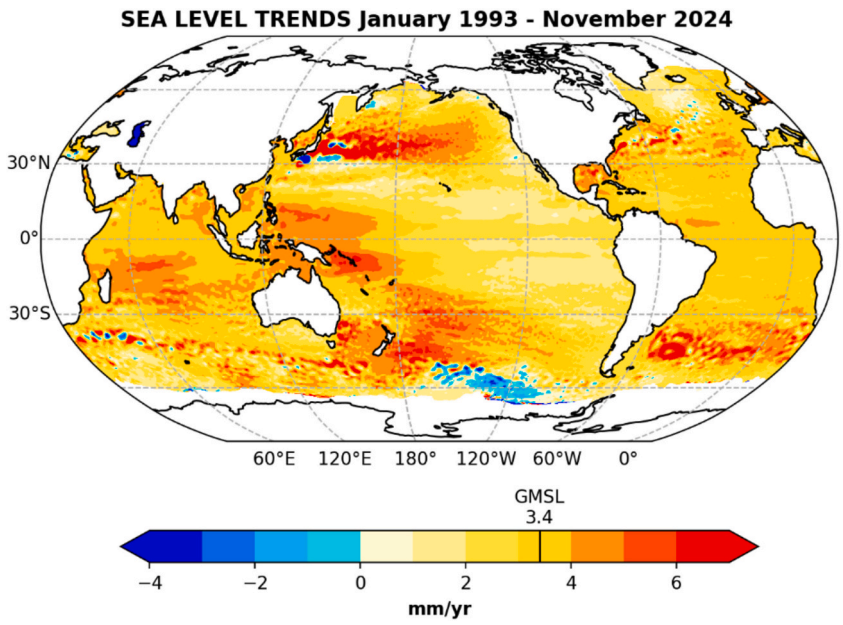

Fig. 1. Spatial trend patterns in sea level over January 1993 and November 2024 from satellite altimetry (data from the Copernicus Climate Change Service, www.climate.copernicus.eu).

In coastal areas, the rate of climate-related sea level change may be different than offshore because it is the combination of the global mean rise and the regional changes, on which the signature of small-scale coastal processes is superimposed. The latter include long-term changes in coastal currents, wind and waves, and seawater density due to variations in freshwater input from rivers (Woodworth et al., 2019). Vertical land motions are additional factors that may cause relative sea level changes to differ substantially from absolute (climate-related) sea level changes in the coastal zones (e.g., Woppelmann and Marcos, 2016).

Several investigations have focused on sea level changes over shelf areas in specific oceanic regions, e.g., Northeast America (e.g., Frederikse et al., 2017, Piecuch et al., 2018, Little et al., 2021, Dangendorf et al., 2023, Camargo et al., 2024), Gulf of Mexico (Wang et al., 2022, Yin, 2023, Steinberg et al., 2024, Leclercq et al., 2025), Northern Europe (e.g., Frederikse et al., 2016; Hermans et al., 2020; Wise et al., 2024), Western Africa (Cisse et al., 2022; Dièye et al., 2023; Ghomsi et al., 2024; Dieng et al., 2021, 2025), Indian Ocean (Han et al., 2019), Southeast Asia (Thompson et al., 2023), etc. The purpose of these studies was to analyze how sea level over shelf areas evolves from monthly to interannual time scale, identify and/or quantify the contribution of local underlying drivers (e.g., river runoff) and estimate the respective importance of ocean mass redistribution on the shelf versus remote steric effects (e.g., Dangendorf et al., 2021). However, the above investigations do not focus on sea level change close to the coast. This is unlike other studies that use tide gauge data, combined with gridded altimetry and model data, to analyze coastal sea level variability on a global scale, this time with the objective of defining coastal regions of coherent interannual variability (e.g., Papdopoulos and Tsimplis, 2006; Han et al., 2019; Royston et al., 2022; Oelsmann et al., 2024). With the exception of the latter studies, the majority of the previous work has focused on regional to large-scale sea level changes and drivers because of limited access to observations of coastal sea level on a global scale. It explains why we still have a limited understanding of processes affecting coastal sea level variations at interannual time scale. But this can now be investigated by exploiting recent developments in coastal altimetry data (e.g., Passaro et al., 2014, 2018; Birol et al., 2021; Benveniste et al., 2020; Cazenave et al., 2022).

This is the main goal of the present study, i.e., investigate and intercompare the dominant structures of interannual variability in coastal sea level and their link with internal climate modes, from both a regional and a global perspective. Another objective is to analyze if these structures change in the cross-shore direction, between the coastline and the open ocean. For that purpose we perform an empirical orthogonal function (EOF) analysis of different data sets: (1) a global sea level dataset at 1132 altimetry-based virtual coastal stations, located at less than 8 km from the coast and homogeneously distributed along the world coastlines (data updated from Benveniste et al., 2020 and Cazenave et al., 2022), (2) gridded altimetry data from the Copernicus Climate Change Service (C3S, www.climate.copernicus.eu), and (3) an ensemble mean of four ocean reanalyses (https://data.marine.copernicus.eu/product/GLOBAL_MULTIYEAR_PHY_ENS_001_031). The study period ranges from January 2002 to June 2021 (a limitation due to the current availability of the altimetry-based virtual coastal station dataset).

Data and methodology are presented in Sections 2 and 3. Section 4 presents the results of the EOF decomposition applied to sea level time series at the altimetry-based virtual coastal stations, globally and regionally. In Section 5 are presented EOF analyses performed in offshore regions using gridded satellite altimetry data, and an ensemble mean of the four ocean reanalyses. Section 6 focusses on the regime shift detected between 2008 and 2012 in coastal sea level. The 6-year cycle found in coastal sea level of several regions is discussed in Section 7. Additional discussion and a conclusion are proposed in Section 8.

2. Data

Different data sets are used in this study.

2.1. Reprocessed altimetry-based coastal sea level data

In the context of the European Space Agency (ESA) Climate Change Initiative (CCI) Coastal Sea Level project (https://climate.esa.int/en/projects/sea-level/), a complete reprocessing of high-resolution (20 Hz, i.e., 350 m resolution along the satellite tracks) along-track satellite altimetry data from the Jason-1, Jason-2 and Jason-3 missions, covering the period January 2002–June 2021 has been performed in the world coastal zones (e.g., Benveniste et al., 2020; Cazenave et al., 2022). The reprocessing uses the altimeter range (i.e., the altitude of the satellite above the sea surface) derived from the Adaptative Leading Edge

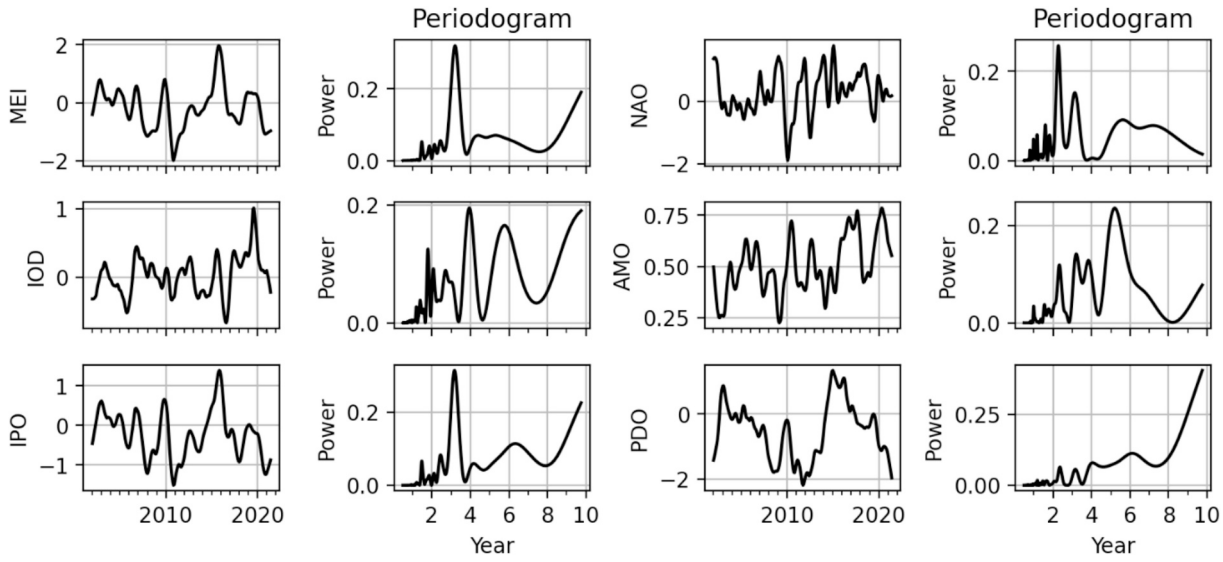

Fig. 2. Time series (over 2002–2021) of MEI, NAO, IOD, AMO, IPO and PDO and associated periodograms. For each climate mode, the time series is shown on the left and the periodogram on the right.

Subwaveform (ALES) retracking method developed by Passaro et al. (2014) to retrieve sea surface height estimates in the coastal zone. The ALES retracking also provides the sea state bias correction used to remove errors in altimetry sea level data due to the presence of ocean waves at the surface. Details of the reprocessing and dataset are described in Benveniste et al. (2020), Birol et al. (2021) and Leclercq et al. (2025). This reprocessing provides altimetry-based sea level time series over 2002–2021 in the world coastal zones (from 50 km offshore to less than 8 km from the coast in global average, with an along-track resolution of 350 m) and the associated sea level trends. Different versions of this dataset have been produced since the beginning of the project, extending its spatial and temporal coverage, and taking into account improvements in the data processing. Here we use the latest validated version of the coastal sea level product (named version 2.4), which provides sea level time series worldwide at 1132 virtual altimetry stations located at less than 8 km from the coast, including 325 virtual stations at less than 3 km from the coast. It is available on the SEANOE website (https://doi.org/10.17882/74354). The virtual stations coverage is that of the Jason satellite tracks where they cross the coast, with an inter-track spacing of ~300 km at the equator, and ~ 150 km at 60° latitude. The virtual stations are located within the 60°N-60°S domain.

2.2. Gridded sea level data from the Copernicus Climate Change Service

We also used a gridded sea level product computed with classical altimetry processing, i.e., the Copernicus Climate Change Service, Climate Data Store, 2018 product with a mesh resolution of 0.25° (https://cds.climate.copernicus.eu/cdsapp#!/dataset/satellite-sea-level-global). The C3S sea level product covers the global ocean and focuses primarily on the recovery of long-term ocean variability. It uses a constellation of two altimeter satellites, with one satellite serving as reference to ensure the long-term stability of the data record and the other used to provide better coverage. The gridded C3S data are available over the altimeter period (1993-present), but here we consider the period from January 2002 to June 2021, as for the virtual coastal stations.

2.3. An ensemble mean of four gridded ocean reanalyses available from the Copernicus Marine Service (CMS)

We used sea surface height data from a Global Ocean Ensemble Reanalysis product provided by CMS (https://data.marine.copernicus.eu/product/GLOBAL_MULTIYEAR_PHY_ENS_001_031). The gridded data are available from 1993 onward (high-precision altimetry era), but as for the other data sets, we focus here on the 2002–2021 time span.

Four ocean reanalyses are used to create the ensemble mean. They include:

- GLORYS2V4 from Mercator Ocean International (Garric and Parent, 2017);
- ORAS5 from the European Center for Medium range Weather Forecast/ECMWF (Zuo et al., 2019).
- C-GLORSv7 from the Euro-Mediterranean Center on Climate Change/CMCC (Storto and Masina, 2016).
- GloSea5 from UK Met Office (MacLachlan et al., 2015).

These products provide different time series (and versions) of 3D global ocean fields at monthly interval. They all use the NEMO (Nucleus for European Modelling of the Ocean) ocean model. Their spatial resolution is 0.25°, i.e., similar to the C3S gridded altimetry data set. GLORYS, ORAS5 and C-GLORS are forced-mode reanalyses. Except GloSea5 (a coupled-mode reanalysis), they assimilate satellite altimetry-based sea level data.

2.4. Time series of internal climate indices

Different climate indices are considered here: MEI (multivariate ENSO Index, https://www.psl.noaa.gov/enso/mei/), PDO (Pacific Decadal Oscillation, https://www.ncei.noaa.gov/pub/data/cmb/ersst/v5/index/ersst.v5.pdo.dat), NAO (North Atlantic Oscillation, https://climatedataguide.ucar.edu/climate-data/hurrell-north-atlantic-oscillation-nao-index-station-based), AMO (Atlantic Multidecadal Oscillation, https://www.ncei.noaa.gov/pub/data/cmb/ersst/v5/index/ersst.v5.amo.dat), IOD (Indian Ocean Dipole, https://www.cpc.ncep.noaa.gov/products/international/ocean_monitoring/indian/IODMI/DMI_month.html) and IPO (Interdecadal Pacific Oscillation, from NOAA ERSST V5, unfiltered, https://psl.noaa.gov/data/timeseries/IPOTPI/).

3. Methods

Regardless of their original temporal resolution, all data sets are transformed into monthly sea level time series. The sea level time series at the 1132 virtual coastal stations are averaged over 10 successive 20

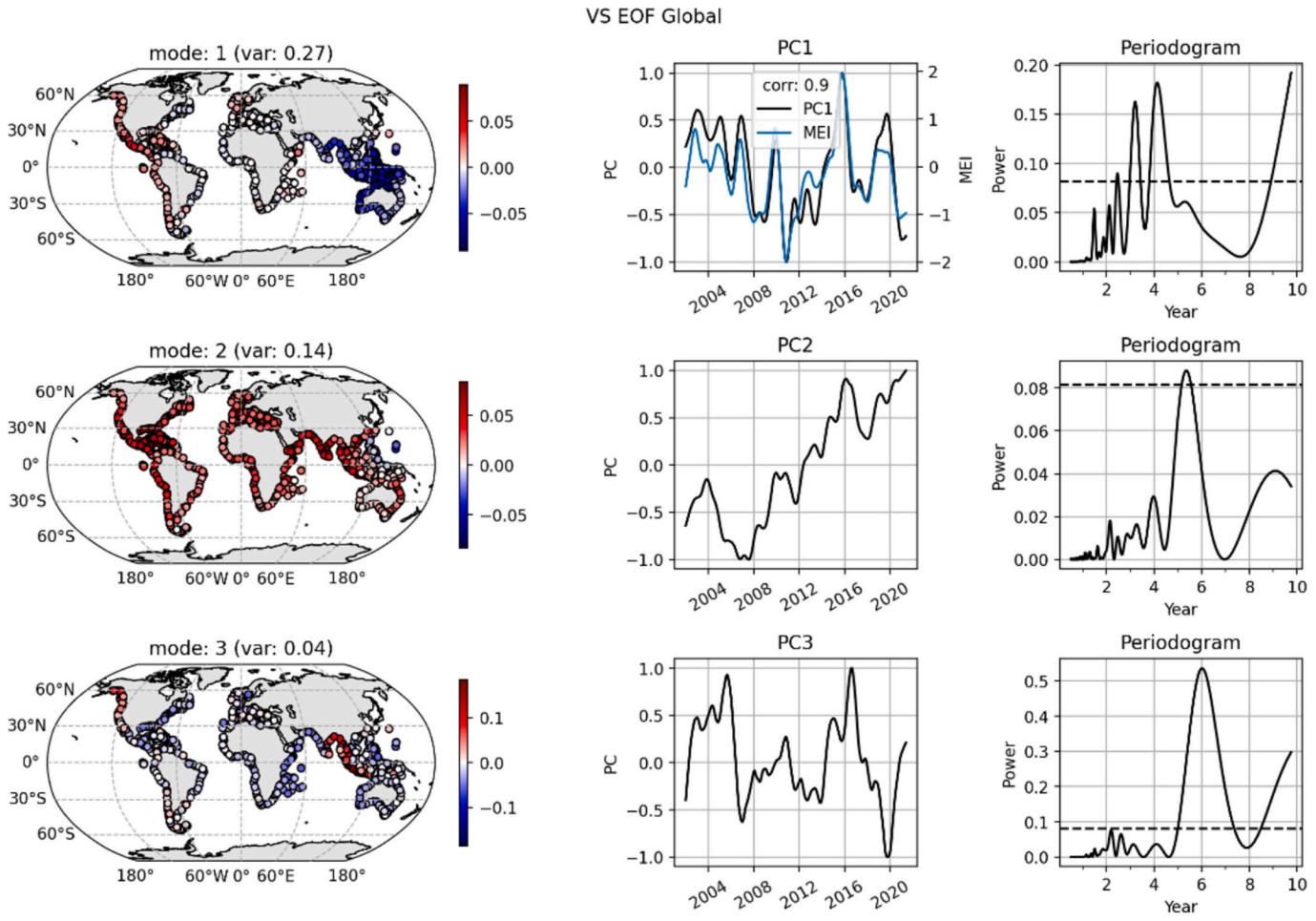

Fig. 3. First three modes of the EOF decomposition of the coastal deseasonalized (but not detrended) sea level time series at the 1132 virtual coastal stations. We show for each mode the spatial distribution (left panel), the corresponding PC time series (middle panel) and the PC periodogram (right panel; the dashed line represents the 90 % confidence level). MEI is superimposed to the PC1 time series. The PCs are normalized and the spatial maps are in meters.

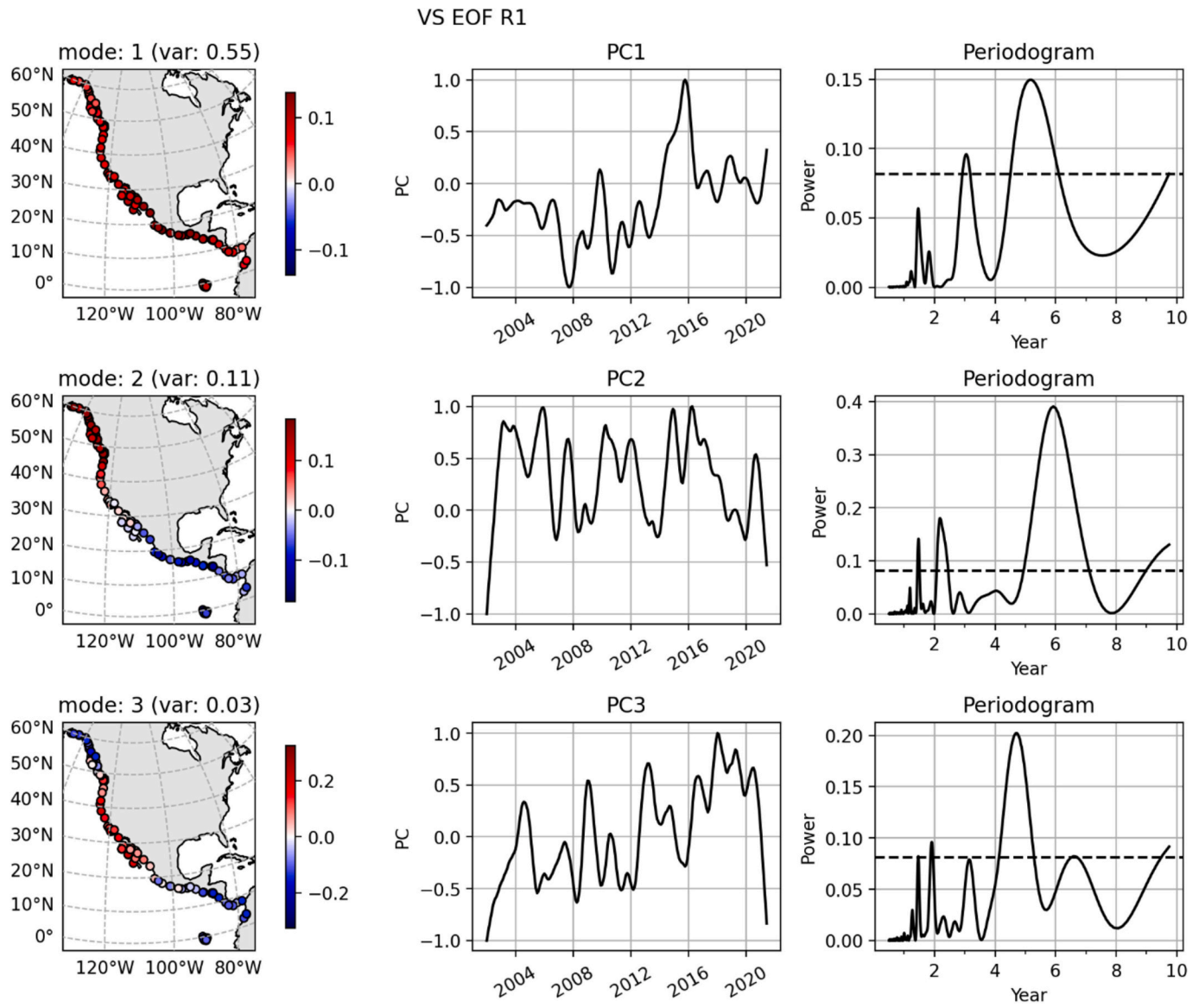

Fig. 4. a: First three modes of the EOF decomposition of coastal sea level time series (deaseasonalized but not detrended) over 2002–2021 for the western coasts of north and central America (R1). For each mode are shown the spatial distribution (left panel), the corresponding PC time series (middle panel) and the PC periodogram (right panel; the dashed line represents the 90 % confidence level). The PCs are normalized and the spatial maps are in meters.
b: First three modes of the EOF decomposition of coastal sea level time series (deaseasonalized but not detrended) for the eastern coasts of north America (R5). For each mode are shown the spatial distribution (left panel), the corresponding PC time series (middle panel) and the PC periodogram (right panel; the dashed line represents the 90 % confidence level). The PCs are normalized and the spatial maps are in meters.
c: First three modes of the EOF decomposition of coastal sea level time series (deaseasonalized but not detrended) over 2002–2021 for the Caribbean region and Gulf of Mexico (R4). For each mode are shown the spatial distribution (left panel), the corresponding PC time series (middle panel) and the PC periodogram (right panel; the dashed line represents the 90 % confidence level). The PCs are normalized and the spatial maps are in meters.
d: First three modes of the EOF decomposition of coastal sea level time series (deaseasonalized but not detrended) over 2002–2021 for Northeast Europe (R6). For each mode are shown the spatial distribution (left panel), the corresponding PC time series (middle panel) and the PC periodogram (right panel; the dashed line represents the 90 % confidence level). The PCs are normalized and the spatial maps are in meters.
e: First three modes of the EOF decomposition of coastal sea level time series (deaseasonalized but not detrended) over 2002–2021 for the Mediterranean Sea (R7). For each mode are shown the spatial distribution (left panel), the corresponding PC time series (middle panel) and the PC periodogram (right panel; the dashed line represents the 90 % confidence level). The PCs are normalized and the spatial maps are in meters.
f: First three modes of the EOF decomposition of coastal sea level time series (deaseasonalized but not detrended) over 2002–2021 for Western Africa (R8). For each mode are shown the spatial distribution (left panel), the corresponding PC time series (middle panel) and the PC periodogram (right panel; the dashed line represents the 90 % confidence level). The PCs are normalized and the spatial maps are in meters.
g: First three modes of the EOF decomposition of coastal sea level time series (deaseasonalized but not detrended) over 2002–2021 for the northern Indian ocean (R11). For each mode are shown the spatial distribution (left panel), the corresponding PC time series (middle panel) and the PC periodogram (right panel; the dashed line represents the 90 % confidence level). The PCs are normalized and the spatial maps are in meters.
h: First three modes of the EOF decomposition of coastal sea level time series (deaseasonalized but not detrended) over 2002–2021 for southeast Asia (R12). For each mode are shown the spatial distribution (left panel), the corresponding PC time series (middle panel) and the PC periodogram (right panel; the dashed line represents the 90 % confidence level). The PCs are normalized and the spatial maps are in meters.

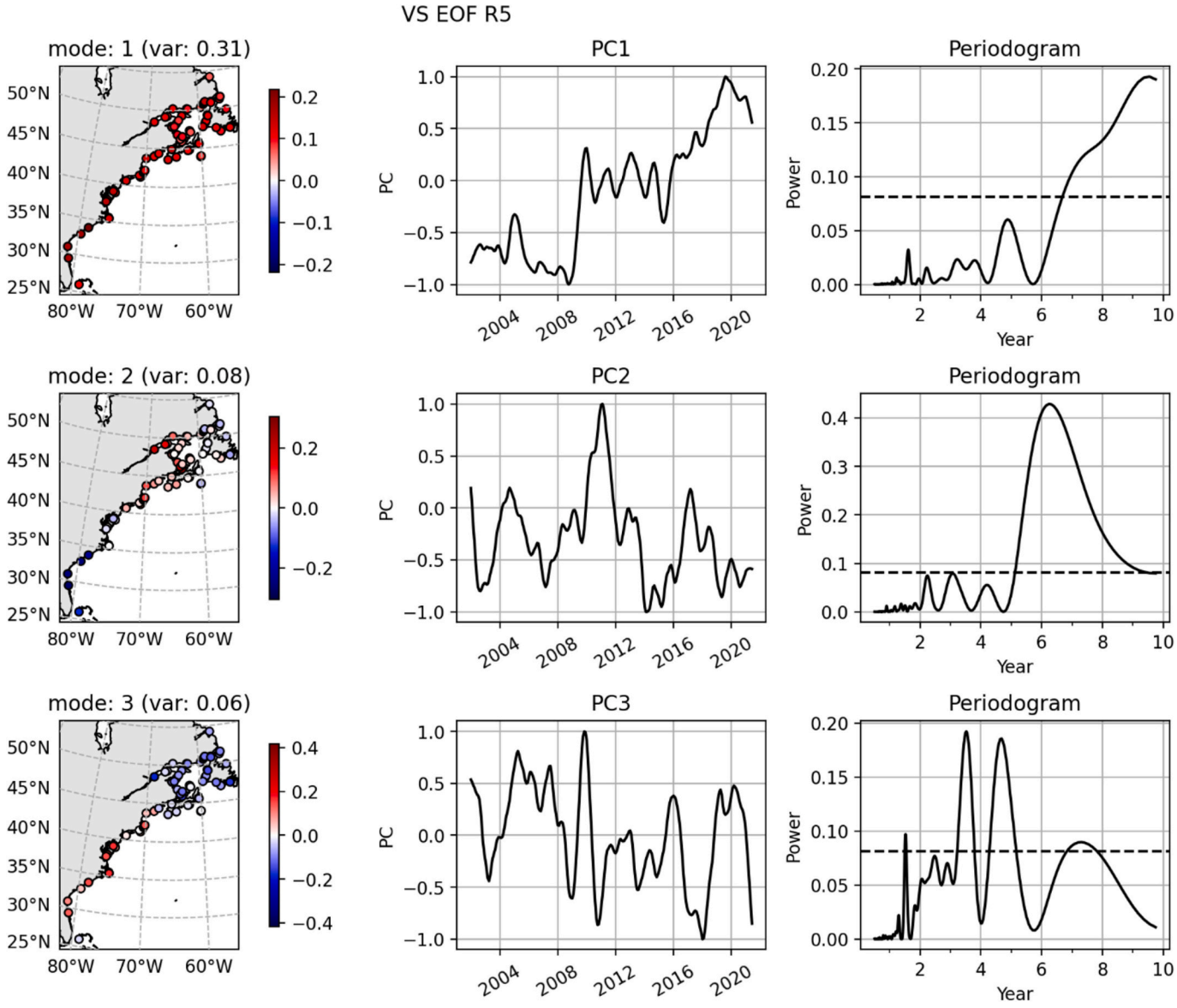

Fig. 4. (*continued*).

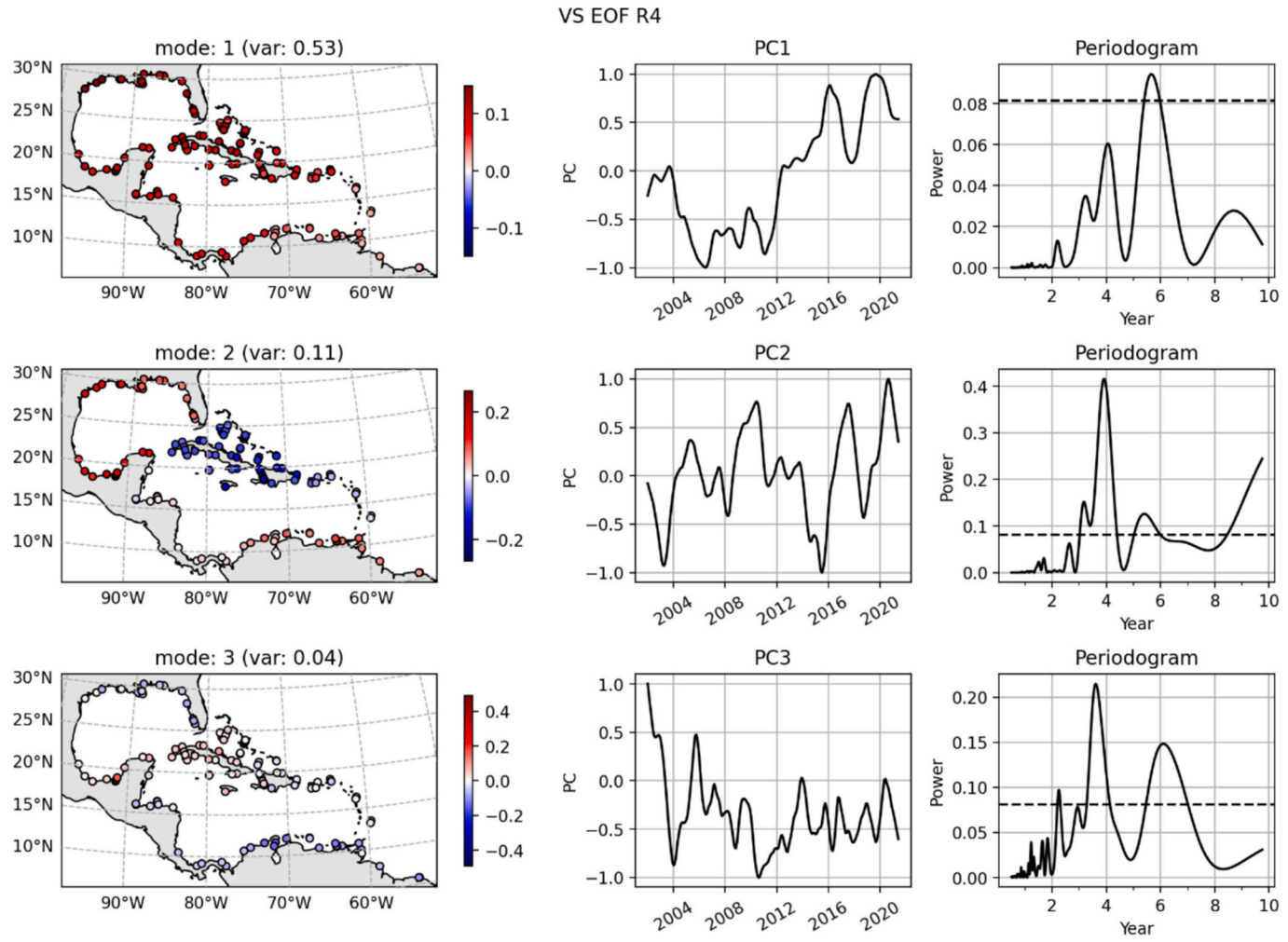

Fig. 4. (*continued*).

Hz (i.e., 350 m) along-track points (hence over a distance of 3.5 km from the first along-track valid point closest to the coast), as explained in Leclercq et al. (2025).

While other approaches could be considered (e.g., Gaussian mixture model as in Oelsmann et al., 2024), the main tool used in this study is the EOF decomposition (Preisendorfer, 1988). This technique is largely used in climate studies to extract spatial patterns of variability and associated temporal evolution.

The EOF decomposition allows to separate a spatially well-resolved signal into spatial modes (EOFs) and their related temporal amplitudes (also called principal components –PCs-).

Conceptually, each EOF is a spatio-temporal pattern of the initial signal that accounts for a percentage of the total variance. The low-order EOFs explain most of the variance and contain the largest spatial scales of the signal. The higher-order EOFs contain smaller spatial scale patterns that are increasingly affected by noise. By construction, EOF spatial patterns and PC of each mode are assumed independent via the hypothesis of mode orthogonality. This condition is however not always verified in physical systems and can be considered as the main limitation of this method.

In the EOF figures presented here, a 12-month smoothing is applied to the PC time series to filter out the high-frequency fluctuations (as we are essentially interested here in interannual variations). The PCs are unitless (normalized by a min-max scaling factor between -1 and $+1$) and the associated spatial maps are in meters, corresponding to the same units of the measured sea level time-series.

We also compute periodograms of the principal components of the EOF decomposition. Periodograms of climate indices are also computed. For that purpose, we use the Lomb-Scargle algorithm (e.g., VanderPlas, 2018).

The seasonal cycle was removed to all data sets using the Multiple Seasonal-Trend decomposition based on the LOESS (MSTL) tool from the statsmodels python library (Bandara et al., 2021). On the other hand, no detrending of the time series is performed. This is done on purpose because the objective of this study is to check how coastal sea level evolves with time, including on the long-term.

4. Results

4.1. Periodograms of the internal climate modes

Because not strictly periodic, it is interesting to quantify in which frequency band the different internal climate modes (i.e., the climate indices) have the maximum of energy during our study period (January 2002 to June 2021), bearing in mind that only periods shorter than 10 years are significant. The MEI, NAO, IOD, AMO, IPO and PDO time series along with their respective periodograms are shown in Fig. 2.

Over the study period, the MEI periodogram is characterized by a strong peak at 3-year. IPO's time series and periodogram resemble those of MEI. PDO is dominated by decadal variations, with a regime change around 2010–2012. NAO displays significant energy between 2.5 and 3 years. Similarly, AMO shows multiple peaks between 2 and 4 years, plus another one close to 5 years. IOD shows a clear 4-year periodicity plus another one around 5.5 year.

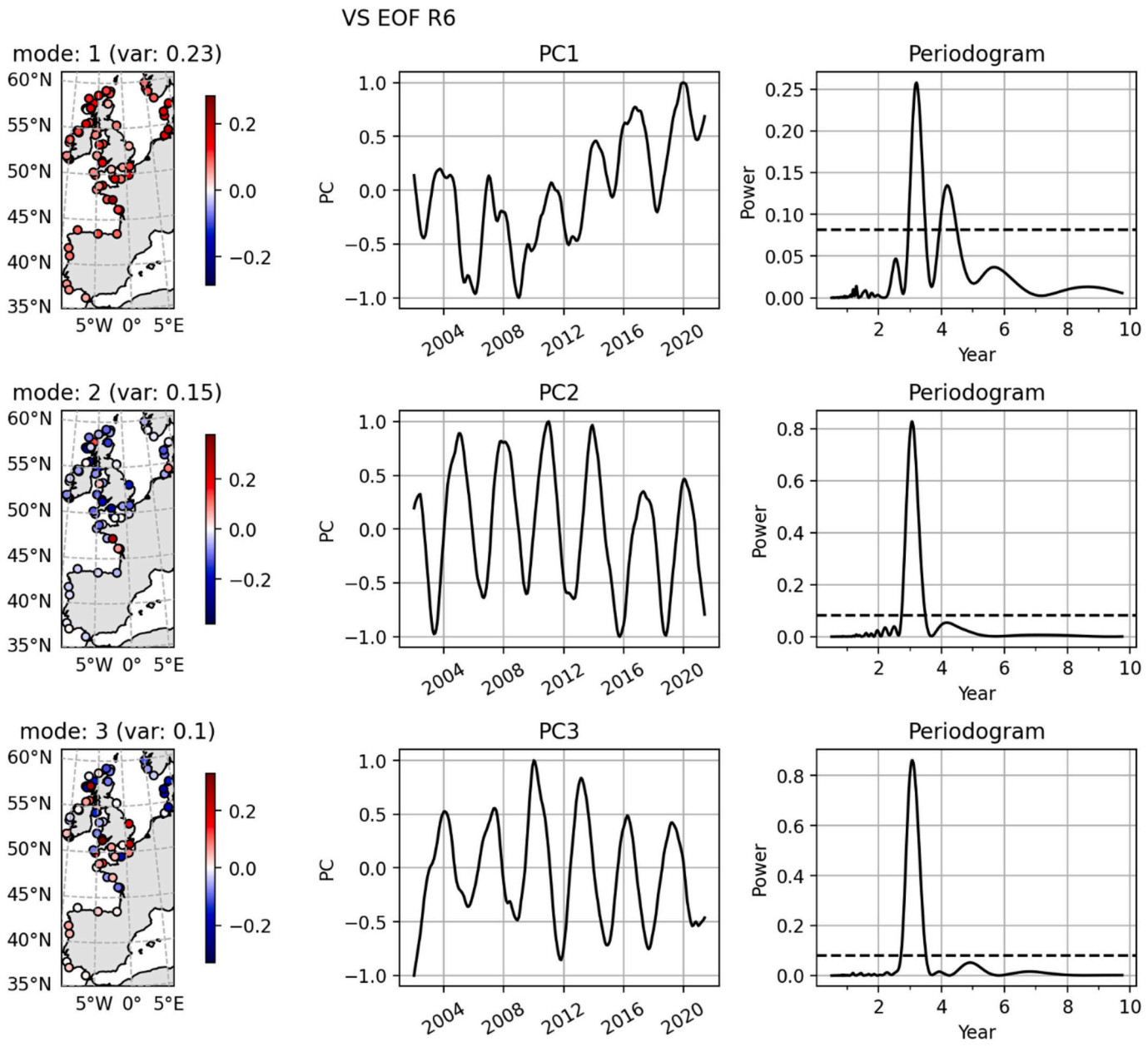

Fig. 4. (*continued*).

4.2. Global EOF decomposition of the sea level time series at the 1132 virtual stations over 2002–2021

Fig. 3 shows the first three modes of the EOF global decomposition of the deseasonalized (but not detrended) sea level time series at the 1132 coastal virtual stations. As a reminder, the latter are all located at less than 8 km from the coast. Fig. 3 shows for each mode the spatial distribution map (left), the principal component time series (PC, middle) and the PC periodogram (right). For the latter, the 90 % confidence level of the peaks is indicated by an horizontal dashed line.

The first mode is clearly dominated by the ENSO signature, mostly seen in the Pacific Ocean, with anti-correlated sea level variations on both sides of the basin. This is illustrated by the high correlation (of 0.9) between the PC1 and superimposed MEI (Fig. 3, top-middle panel). In the other oceanic coastal regions, this mode has a low signature. Because of the strong global influence of ENSO, the effect of other climatic modes (e.g., NAO or AMO in the Atlantic Ocean) is hardly visible on mode 1 of the global analysis.

The second mode shows a long-term positive trend in coastal sea level after 2008, on which are superimposed short-term oscillations around 4–5-year periods. Interestingly, the mode 2 positive trend beyond 2008 is seen in most coastal regions except on the Pacific side of southeast Asia where the trend is slightly negative. The peaks at 4-5 years are not significant.

Although its explained variance is low, the third mode reveals a clear 6-year periodicity in coastal sea level (well above the 90 % confidence level), in particular along the coasts of the northeast Pacific and eastern Indian Ocean. It could be related to the 6-year cycle which has been recently discovered in several climate parameters (Cazenave et al., 2023, 2025; Pfeffer et al., 2023). A dedicated discussion on this topic is provided in Section 7.

4.3. EOF decomposition of coastal data in specific regions

We present below results of the EOF decomposition of the sea level time series over January 2002–June 2021 at the virtual coastal stations,

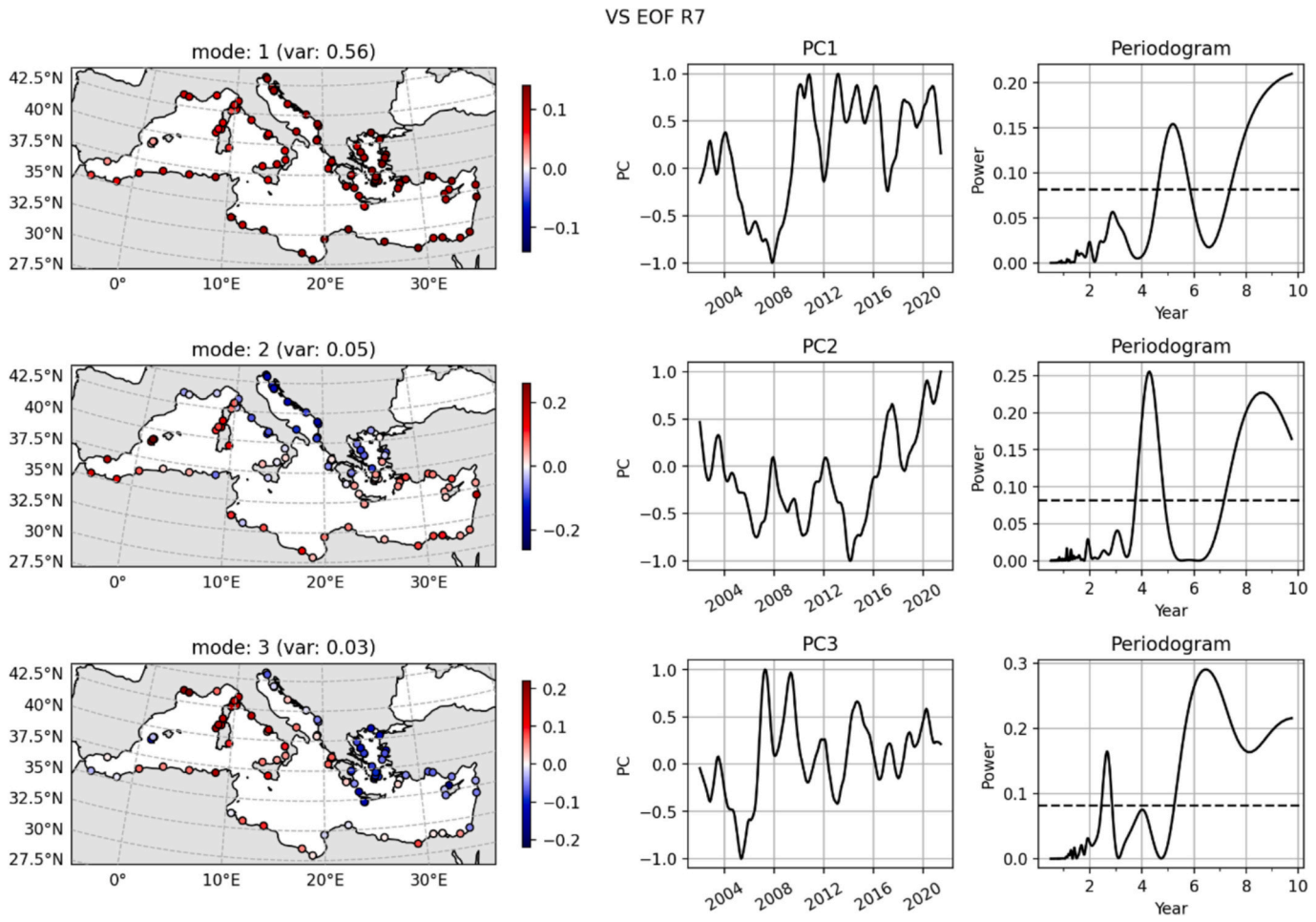

Fig. 4. (*continued*).

but now performed at a regional scale (Figs. 4a-h). Because of regional differences in ocean dynamics and non-uniformity of impacts of climate modes, the interannual variability of coastal sea level is expected to vary from one region to another. We focus below on eight coastal areas (western coasts of North & Central America, Northeast coast of America, Caribbean region and Gulf of Mexico, Northwestern Europe, Mediterranean Sea, Western Africa, North Indian Ocean and Southeast Asia).

4.3.1. *Western coasts of North & Central America (region R1)*

Fig. 4a shows the first three modes of the EOF decomposition of coastal sea level time series for the western coasts of north and central America.

The first mode explains now 55 % of the variance (in comparison to 27 % in the global scale analysis). The signature of the IPO and AMO (peaks at ~3 and 5 years respectively) is also visible. Modes 2 and 3 have much lower explained variance. What is noticeable is that the 6-year cycle has now moved to mode 2 compared to the global analysis where it was present in the 3rd mode. Its impact on sea level is dominant between 40°N and 60°N. Mode 3 explains much less of the regional coastal sea level variability (3 % explained variance) and has a significant 4.5-year cycle.

4.3.2. *Northeast coast of America (region R5)*

Along the northeast coast of America, mode 1 largely dominates the sea level variability, with 31 % of the explained variance and a coherent spatial structure along the coast (Fig. 4b). It shows a large step change around 2010, with higher sea level beyond that date. It is worth noting that mode 2 (8 % of the variance) displays a significant 6-year cycle, particularly significant north of 40°N. Mode 3 (6 % of the variance) has a slightly bimodal structure along the coast and is associated to different peaks of energy (around 3 and 5 years).

4.3.3. *Caribbean region and Gulf of Mexico (region R4)*

Mode 1 of Fig. 4c shows the same behavior as observed in mode 1 for Northeast America, i.e., a regime change around 2012, slightly later than along the Northeast American coast, and with a larger explained variance (53 % versus 31 %). A significant peak at 4 years is seen in mode 2 (11 %) of the variability) suggestive of a remote influence of the IOD. This mode shows opposite amplitudes in sign between the Caribbean islands and the rest of the region. Mode 3 explains much less of the variability (4 %) associated with peaks around 4 and 6 years.

4.3.4. *Northwestern Europe (region R6)*

The PCs of modes 1, 2 and 3 (Fig. 4d), 23 %, 15 % and 10 % of explained variance respectively, all show a clear 3-year period fluctuation which is likely the signature of the NAO, but with possibly a remote influence of ENSO. The EOF analysis was not able to clearly separate this signal from the rest of the interannual variability in this region. In addition, mode 1 shows the same long-term behavior as observed on the other side of the Atlantic, i.e., a regime change between 2008 and 2012. As above, it shows a coherent spatial structure all along the coast, whereas modes 2 and 3 are much more complex.

4.3.5. *Mediterranean Sea (region R7)*

In the Mediterranean Sea (Fig. 4e), mode 1 dominates, with an explained variance of 56 % and, here again with a homogeneous spatial

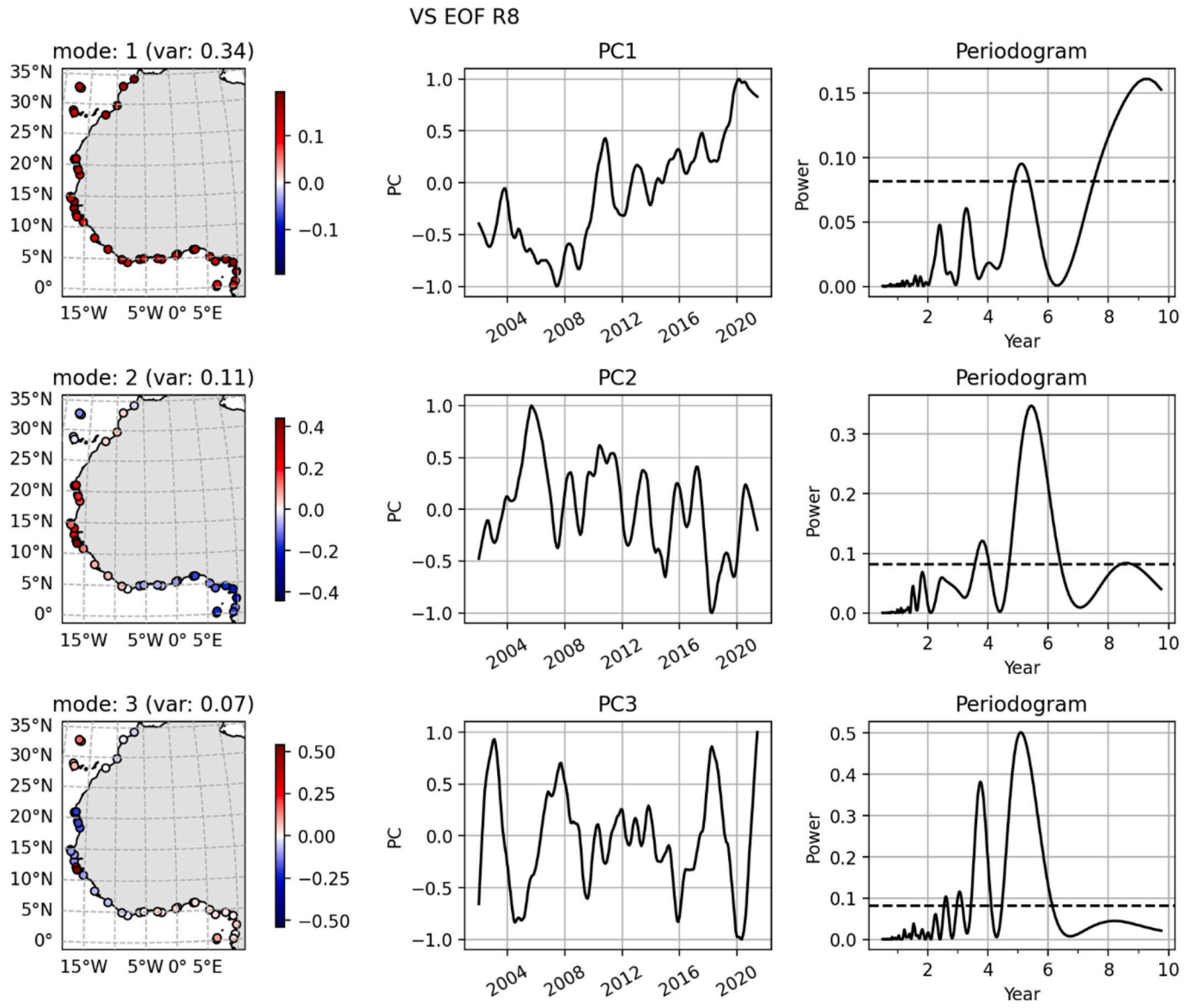

Fig. 4. (*continued*).

structure. It is a combination of a trend, with a regime change between 2008 and 2010, and interannual fluctuations with period around 5 years. Modes 2 and 3 have very small explained variance (5 % and 3 % respectively).

4.3.6. Western Africa (region R8)

The western coast of Africa again presents the same behavior as previously mentioned for northeast America and northwestern Europe, i.e., the regime change between 2008 and 2010 which dominates the coastal sea level variability, with a coherent spatial structure all along the coast (Fig. 4f). The AMO influence is also visible in both modes 2 and mode 3 through a significant peak around 5 years.

4.3.7. North Indian Ocean (region R11)

Again, mode 1 for the North Indian Ocean shows the regime shift between 2008 and 2012, previously seen in the other regions, but this time explaining 41 % of the coastal sea level variability at interannual scale (Fig. 4g). It also shows the influence of IOD (peak around 4 years). Mode 2 (18 % of the explained variance) displays high frequency fluctuations in addition to a 6-year cycle along eastern Indian coasts and Gulf of Bengal. Mode 3 is lower (8 % of explained variance) and associated to a sharp increase in coastal sea level in 2012, here again in the eastern part of the study region.

4.3.8. Southeast Asia (region R12)

Mode 1 dominates the regional coastal sea level variability, with 52 % explained variance. It is dominated by the combined effects of ENSO and IOD (peaks between 2 and 4 years), affecting the whole region (Fig. 4h). Interestingly, mode 2 (8 % of the variability) displays a 6-year cycle, mostly significant along the Indian coasts of Indonesia. Mode 3 (3 % of the total variance) is marginally significant.

4.4. Synthesis of the coastal sea level EOF results

From the results presented above, we note an important regional signature in coastal sea level of some climate modes. This is by no means a new finding, as it has already been reported in several previous studies (e.g., Papdopoulos and Tsimplis, 2006; Han et al., 2019; Oelsmann et al., 2024). For example, using gridded altimetry data, Oelsmann et al. (2024) identified nine clusters of coherent interannual sea level variability along the world coastlines, sometimes highly correlated with internal climate modes.

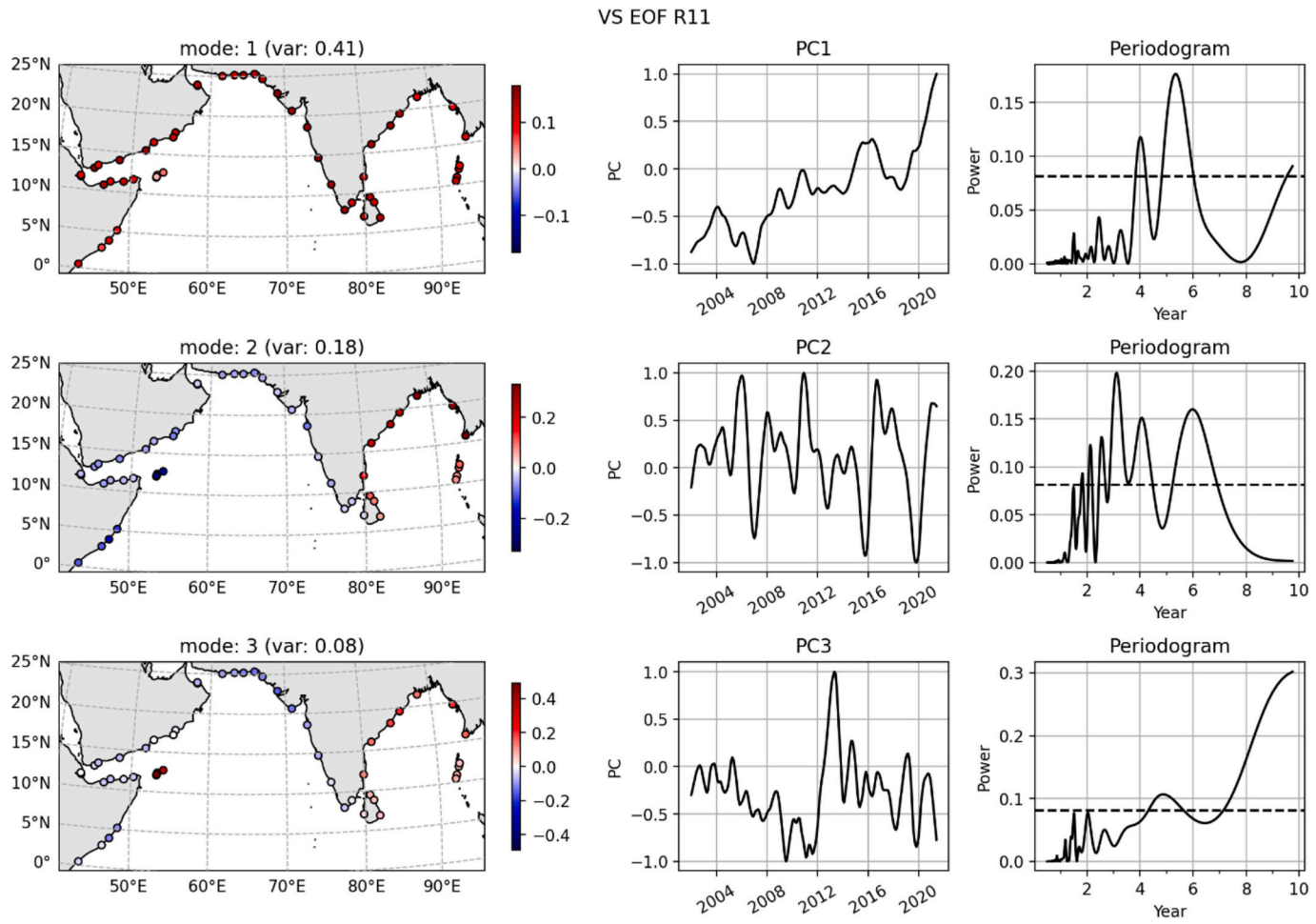

Fig. 4. (*continued*).

On the other hand, the present analysis detects a regime shift in coastal sea level between 2008 and 2012, in all regions. This will be discussed in more detail in Section 6. Similarly, the detection of a 6-year cycle in sea level in some coastal regions is new. It will be discussed in Section 7.

Table 1 below summarizes the main features derived from the above analysis depending on region.

5. EOF decomposition of offshore sea level data

To understand to what extent the characteristics of the interannual variability of coastal sea level captured in the virtual station dataset (Section 4) are related to the one located further offshore, we perform similar EOF decompositions of offshore gridded sea level data, over the time span 2002–2021, using successively the C3S altimetry data set and an ensemble mean of ocean reanalyses. For that purpose, three cases are considered in both cases: only data located between 0 and 50 km, 50–100 km and then 100–500 km from the coast.

5.1. Gridded C3S altimetry data

Results for the three offshore domains are shown in Figs. 5a–c. Note that the coverage of the gridded data is slightly larger than in the virtual station case because the dataset has a resolution of 0.25° and covers the high latitude regions above 60°N.

Comparing Figs. 3 and 5a–c, we note that modes 1 of the virtual stations and gridded data (0-50 km, 50-100 km and 100-500 km cases) compare well, showing that the interannual variability is present in both coastal and offshore sea level. It also confirms the worldwide influence of ENSO. The modes 2 of the three gridded cases also show the same trend change between 2008 and 2012 as the virtual station case: positive along most coastlines except in a narrow band on the Pacific side of southeast Asia, where it has an opposite sign. Mode 3's periodograms of the 0-50 km and 50-100 km cases show a peak at 6 years, while for the 100–500 km case, the peak is shifted at ~7 years. Explained variances of mode 1 is relatively similar in the 0-50 km and 50-100 km cases and then decrease further offshore. If the dominant EOF modes appear to be almost the same as the distance to the coast increase, their respective importances in the coastal sea level variability seem to change.

5.2. EOF decomposition of the ocean reanalyses

In order to compare the altimetry-based observations with model outputs, we performed an EOF analysis of the gridded reanalyses ensemble mean. As for the C3S gridded altimetry data, three cases are considered here: only data located in the 0-50 km band from the coast, and in the 50-100 km and 100–500 km bands offshore. Below, we only present the 0-50 km case (Fig. 6). Here again, the data are deseasonalized but not detrended before analysis.

The spatial structures and respective importance of the three EOF modes are similar to those obtained with C3S altimetry data. However, the temporal evolution of modes 2 and 3 is different. It may reflect variability between the individual numerical solutions on which the ensemble mean is constructed. Mode 1 (28 % of the explained variance) is strong in the tropical Indo-Pacific region. It is characterized by a positive trend as of 2010–2012. The PC1 periodogram displays different

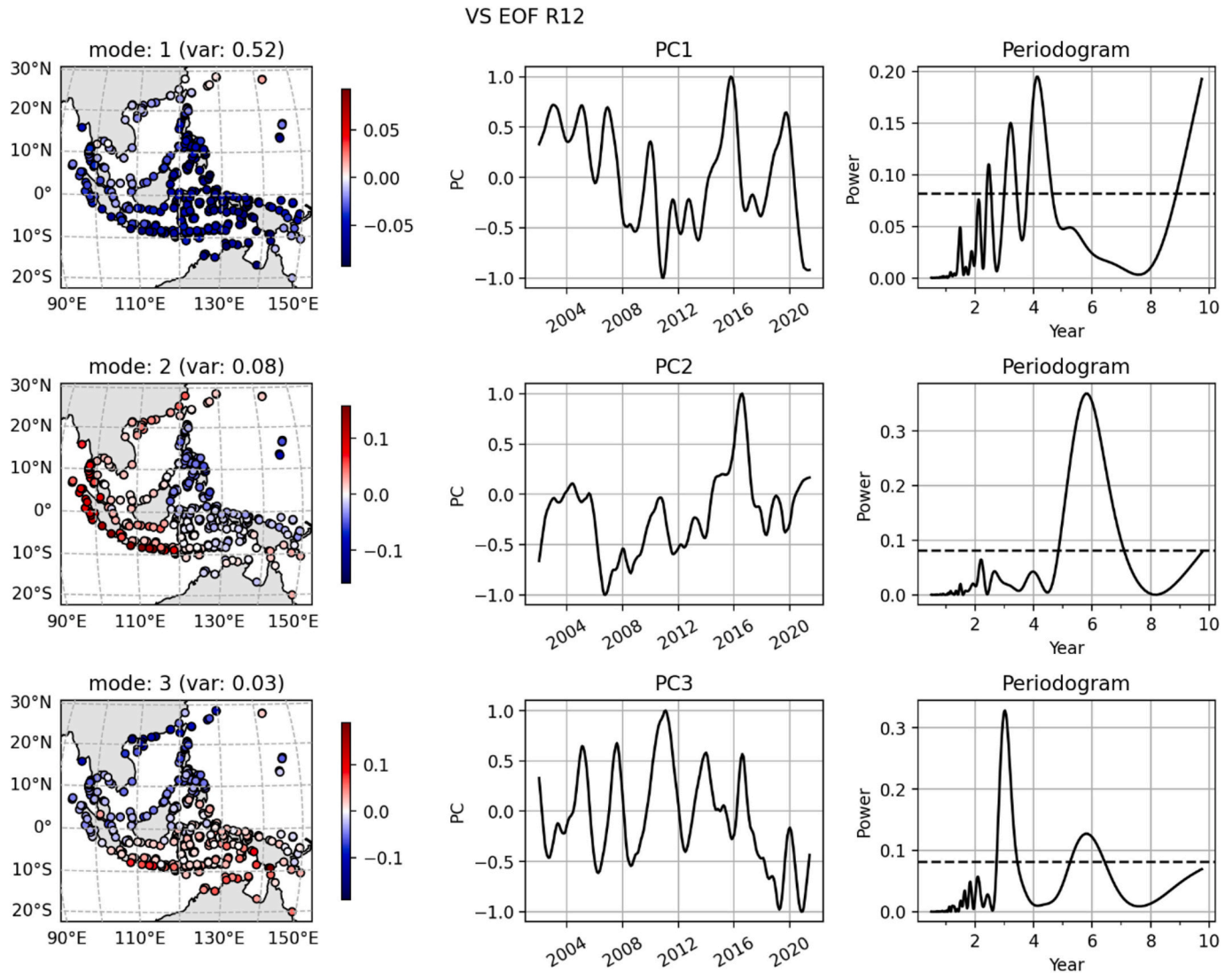

Fig. 4. (*continued*).

Table 1
Main features derived from the EOF analysis in the eight studied coastal regions.

Coastal Region	Climate modes	Regime shift between 2008 and 2012	6-year cycle
Northwest & central America	IPO	yes	yes
Northeast America	NAO, AMO	yes	yes
Caribbean & Gulf of Mexico	ENSO, IPO, IOD	yes	/
Northeast Europe	NAO	yes	/
Mediterranean Sea	AMO	yes	/
Northwest Africa	AMO	yes	/
North Indian Ocean	ENSO, IOD	yes	yes
Southeast Asia	ENSO, IOD	yes	yes

peaks in the 2–4-year waveband, likely a combined effect of MEI/ENSO, NAO and IOD (not well separated by the EOF method and only slightly above the noise level). Mode 2 (17 % of the explained variance) has an almost global signature, with a dipole between the tropical Indo-Pacific region and the rest of the world coasts. Mode 3 (8 % of the explained variance) shows some energy around 6-year. However, the 6-year peak is better resolved in the EOF decomposition of data in the 50-100 km band (not shown). The regime shift between 2010 and 2012 is well seen in the reanalyses and in the gridded altimetry data.

6. A regime shift in sea level around 2008–2012?

The EOF analyses presented above, suggest that a quasi-step change in coastal/near coastal sea level occurred in many regions during the 2008–2012 time span. It is worth noting that this regime shift is also seen at the same date at the virtual coastal stations of Southeast America and Southwest Africa (both on the Atlantic sides of these continents) (EOFs not shown). At the virtual coastal stations, it occurs around 2008–2010 in the following regions: Northeast and Southeast America, Gulf of Mexico, Mediterranean Sea, Western Africa, Indian Ocean. In the offshore sea level data (e.g. both gridded altimetry and reanalyses), it seems to be slightly delayed in time (around 2010–2012). When the ENSO signal is removed from the gridded altimetry data located in the 0-50 km band from coast (removing mode 1 of the previous EOF decomposition), this regime shift is well seen around 2012 in the first mode of the new EOF decomposition (not shown). Interestingly, if we now compute the EOF analysis at global scale, using gridded C3S altimetry data, such a regime shift is also well visible (Fig. 7). Mode 1 shows a clear increase in sea level rate around 2012 in all oceanic domains (except in a narrow elongated band located next to the Philippines Sea where the trend is negative). In modes 2 and 3, the signature of ENSO

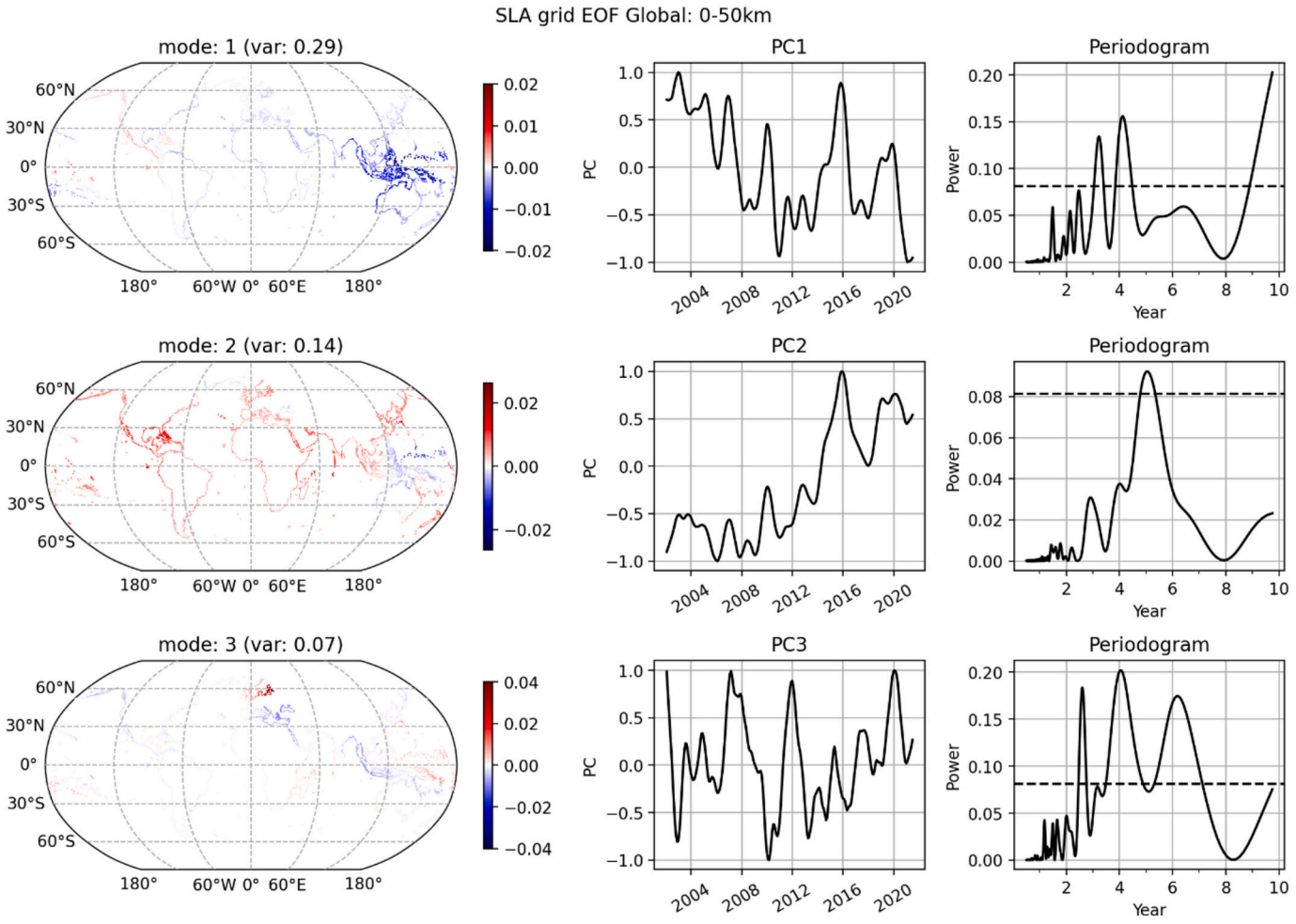

Fig. 5. a: PC time series over 2002–2021 of modes 1, 2 and 3 and associated periodograms of the EOF decomposition of C3S gridded altimetry data (deseasonalized but not detrended) in the 0-50 km band from the coast. For each mode are shown the spatial distribution (left panel), the corresponding PC time series (middle panel) and the PC periodogram (right panel; the dashed line represents the 90 % confidence level). The PCs are normalized and the spatial maps are in meters.
b: PC time series over 2002–2021 of modes 1, 2 and 3 and associated periodograms of the EOF decomposition of C3S gridded altimetry data (deseasonalized but not detrended) in the 50-100 km band from the coast. For each mode are shown the spatial distribution (left panel), the corresponding PC time series (middle panel) and the PC periodogram (right panel; the dashed line represents the 90 % confidence level). The PCs are normalized and the spatial maps are in meters.
c: PC time series over 2002–2021 of modes 1, 2 and 3 and associated periodograms of the EOF decomposition of C3S gridded altimetry data ((deseasonalized butnot detrended) in the 100-500 km band from the coast. For each mode are shown the spatial distribution (left panel), the corresponding PC time series (middle panel) and the PC periodogram (right panel; the dashed line represents the 90 % confidence level). The PCs are normalized and the spatial maps are in meters.

dominates.

In order to not only rely on visual inspection of the figures, we applied a statistical method to more precisely locate in time the regime shift. For that purpose, we used the Bayesian Estimator of Abrupt change, Seasonal change and Trend (BEAST) tool developed by Zhao et al. (2019). This method allows to detect changes in trend in time series using Bayesian algorithms. The BEAST method is applied here to the mode 2 PC of the EOF decomposition of the coastal sea level at the 1132 virtual stations (Fig. 3). The minimum separation time interval (called trend length) between to neighboring trend changes is an entry that depends on the type of the analysis to be performed. Being interested here in the interannual variability, we tested three cases: 5 years, 7 years and 9 years for the chosen trend length. Results are shown in Fig. 8.

Fig. 8 clearly shows that PC2 of the EOF decomposition of the virtual station sea level displays a change in trend within the 2008–2012 time interval.

It is worth mentioning that several previous studies have found evidence of an abrupt change in sea level between 2008 and 2012 in some coastal regions, with higher sea level beyond that date, e.g., along the coast of southeast US and Gulf of Mexico (Dangendorf et al., 2023; Yin, 2023; Steinberg et al., 2024; Leclercq et al., 2025), as well as a regime shift in sea level trend (turning from positive to negative) in the south China Sea around 2009 (Cheng et al., 2023; see also Qu et al., 2023). Cheng et al. (2023) elaborate on the South China Sea regime change, linking the regional sea level response to the PDO whose phase changed around 2010–2012. According to these authors, this caused a weakening of trade winds at the equator compared to the previous decade.

We cannot exclude that the regime shift seen in coastal sea level is a more global phenomenon that has impacted the climate system. For example, a climatic regime shift around 2010 has been reported by Amano et al. (2023) in Northeast Eurasia, possibly linked to a change in the Arctic Oscillation. A large increase in coastal ice mass loss in West Antarctica as of 2009 was observed by Zwally et al. (2021) and a shift in ocean heat content of the southern oceans around 2012 was reported by Wang et al. (2021). These shifts seem to be related to a change in the phase of the PDO, as illustrated in Fig. 2. It may be worth to recall that a PDO shift occurred in 1976/1977 which had large scale impacts on

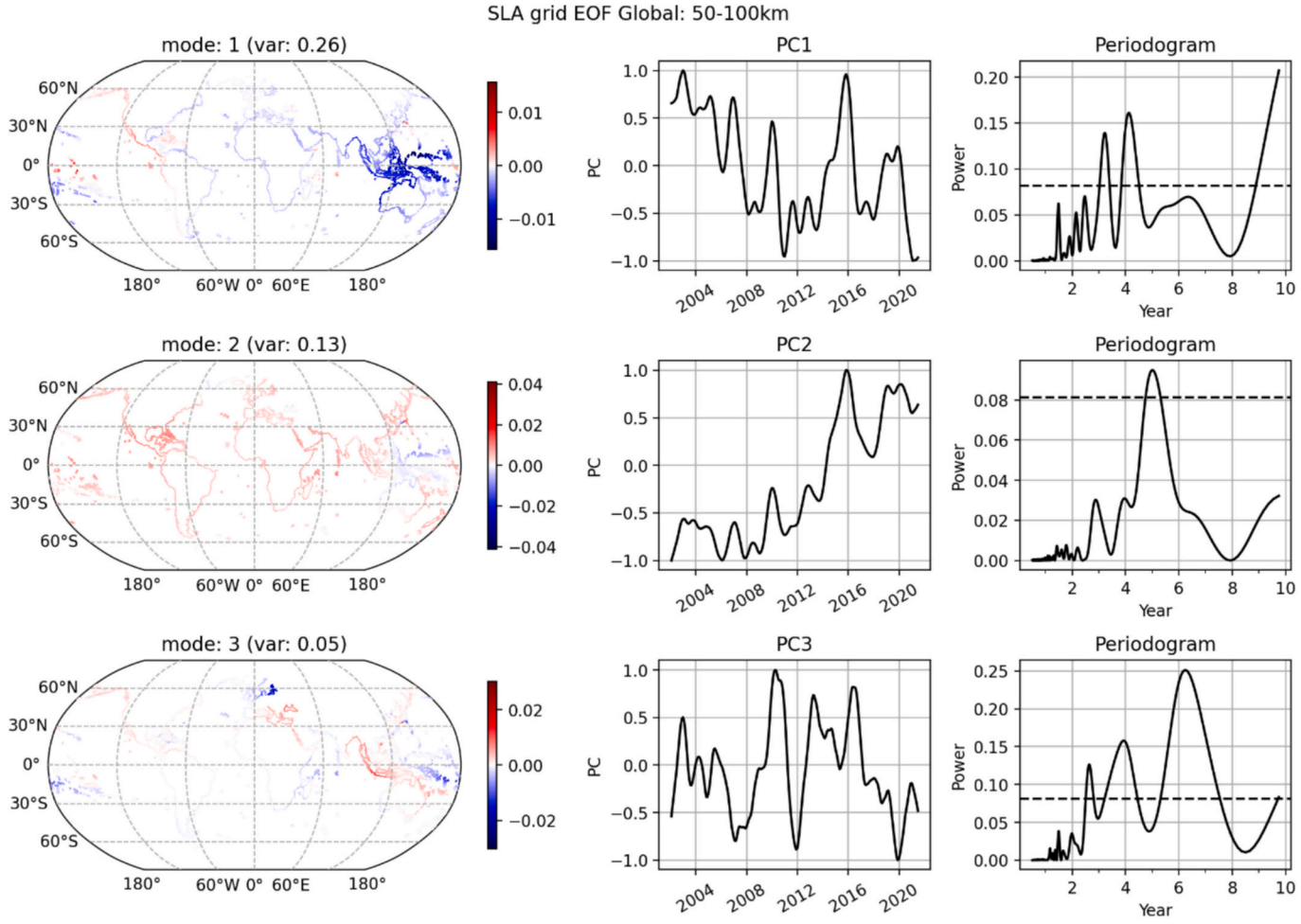

Fig. 5. (*continued*).

climate (Miller et al., 1994; Hartmann and Wendler, 2005; Wu et al., 2005). Such PDO phase shifts are supposed to be linked to the decadal variability of the atmosphere-ocean system in the tropical Pacific (Lyu et al., 2017; Power et al., 2021; Wang et al., 2021). However, we cannot also exclude that an increase in anthropogenic radiative forcing also played a role (e.g., Hodnebrog et al., 2024).

Returning to sea level, it seems that some change in the global mean sea level (GMSL) is also visible around 2010, as illustrated in Fig. 9.

While the temporal evolution of the GMSL shown in Fig. 9 is usually interpreted as an acceleration classically expressed by a quadratic trend (e.g., Dieng et al., 2017; Nerem et al., 2018; Guérou et al., 2023; Hamlington et al., 2024), we cannot exclude that it would either be explained by two linear trends, with a change in slope around 2010. Over 1993–2009, the slope is estimated to 2.65 ± 0.3 mm/yr and to 4.43 ± 0.3 mm/yr over 2010–2024.

7. The 6-year cycle observed in sea level along some coastlines

A cycle of about 6-year has been found in some parameters of the Earth system, e.g., in the rotation of the solid Earth (e.g., Abarca del Rio et al., 2000 and many subsequent publications), in the internal magnetic field (Currie, 1973, Mandea et al., 2012, 2015), in fluid core motions (Gillet et al., 2010, 2022), in GNSS-based crustal deformations (Watkins et al., 2018), in the Earth's oblateness (Chao and Yu, 2020) and in other low-frequency terms of the Earth's gravity field (Mandea et al., 2015). Recently, a 6-yr cycle has also been detected in several parameters of the climate system (Cazenave et al., 2023; Pfeffer et al., 2023). This the case in particular for the rate of change of the GMSL and some components of the GMSL (e.g., glacier and Greenland ice mass loss) (Moreira et al., 2021). A 6-yr cycle has also been detected in precipitation data, in GRACE-based terrestrial water storage and in global hydrological models, (Pfeffer et al., 2023). In addition, it has been observed in the zonal wind circulation of the atmosphere and in its angular momentum (Pfeffer et al., 2023). Finally, the Earth's mean surface temperature also displays a clear cycle at 6-year period, dominant in the Arctic region, as well as the global mean ocean heat content (Pfeffer et al., 2023; Cazenave et al., 2025). While the 6-year cycles of the magnetic field and solid Earth rotation are known for long and are convincingly attributed to Earth deep interior processes occurring in the core and at the core-mantle boundary (e.g., Gillet et al., 2022), the 6-year cycle in the climate system is a recent discovery. It implies that the whole Earth system is oscillating with a 6-year periodicity. Cazenave et al. (2025) reviewed the 6-year cycle affecting the whole Earth system and proposed different mechanisms potentially able to explain the observations. However, the question remains open.

The fact that the coastal sea level data display a clear 6-year cycle, only in some regions, adds another puzzling element to this question. The 6-year cycle found in coastal sea level north of 40°N along the western and eastern coasts of North America could eventually be linked to the observed 6-year cycle in Arctic surface temperature (via thermal expansion and Greenland melting). On the other hand, the observed 6-year cycle in sea level in the Northeast Indian Ocean and along the Indian coasts of Indonesia could be driven by coastal winds if the latter exhibit such a 6-year oscillation. But what is the global origin of this cycle in all the zones where they are observed? It is beyond the scope of the present study to investigate this question in more detail. But the

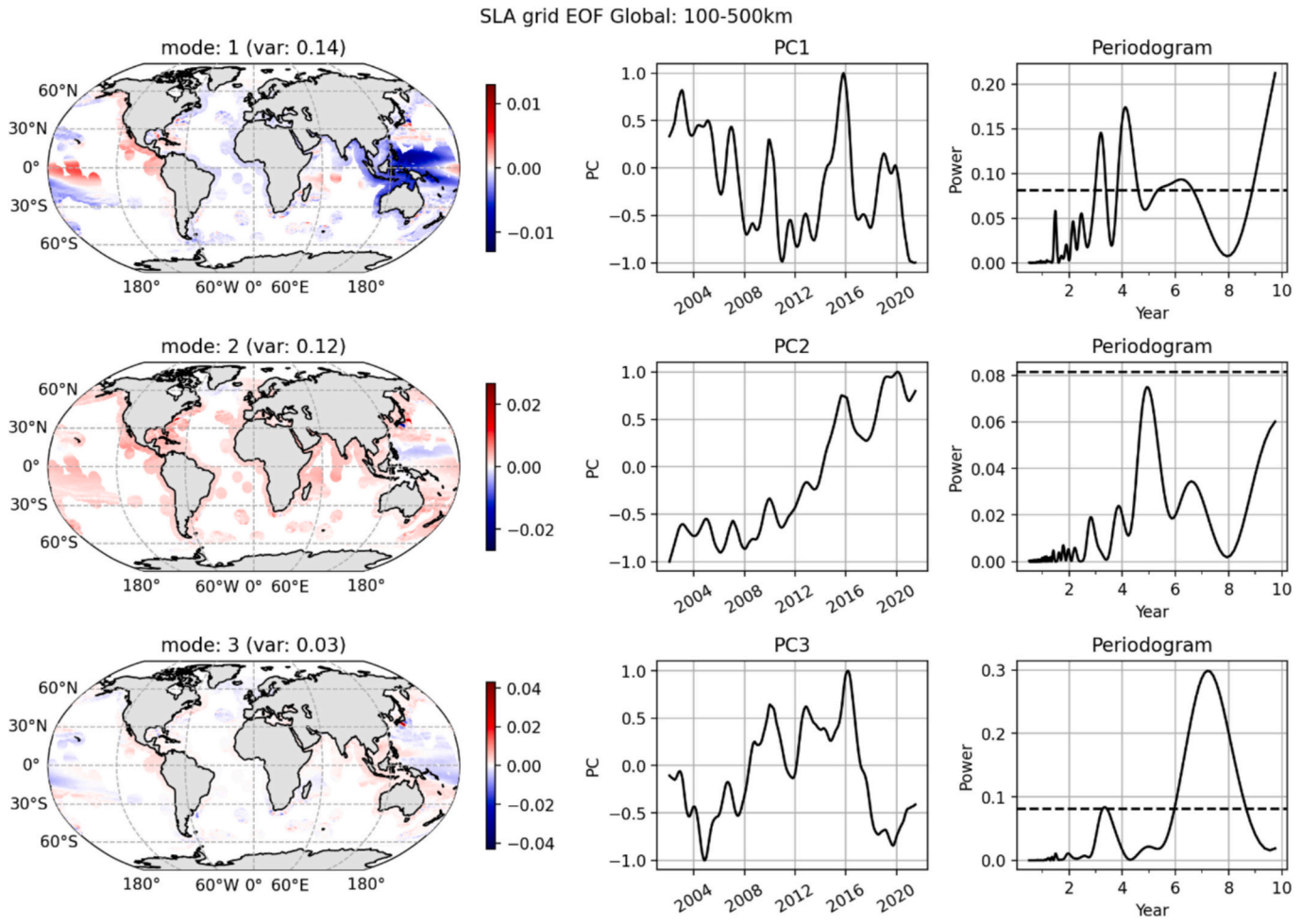

Fig. 5. (*continued*).

discovery of this new signal in observed coastal sea level of some regions and the fact that it is also captured in ocean reanalyses should enable us to make progress in the future in characterising and understanding it.

8. Discussion and conclusion

In Section 4 we reported interannual variations of coastal sea level that are related to internal climate indices. As shown by many studies, internal climate modes represent the dominant factors of interannual to multidecadal variability of oceanic parameters, including sea level. This mostly results from ocean-atmosphere interactions and associated feedback mechanisms. Focusing on the interannual time scale, the most prominent mode of variability is related to ENSO, affecting dominantly the Pacific Ocean but with strong influence on remote regions via inter-basin teleconnections caused by modifications of the Walker and Hadley atmospheric circulations (e.g., Yu et al., 2020, An and Wang, 2020, Chang et al., 2020, Rodriguez-Fonseca et al., 2020). Other modes of interannual variability affect other oceans, e.g., NAO and AMO in the Atlantic Ocean (Rodriguez-Fonseca et al., 2020) and IOD in the Indian Ocean (Kucharski et al., 2020), to just quote a few. As reviewed in detail in Mechoso (2020), important inter-basin interactions take place at interannual time scales through oceanic and atmospheric connections, which explains why in a number of cases, the remote signature of some climate modes is noted.

Several previous studies have compared the interannual variability of coastal sea level with internal climate modes, either using tide gauge data (e.g., Papdopoulos and Tsimplis, 2006; Han et al., 2019) or gridded altimetry data (Oelsmann et al., 2024). These studies highlighted the well-known influence of MEI/ENSO along the eastern Pacific coasts, of NAO and AMO in the Atlantic and of the IOD in the Indian Ocean.

As mentioned in the introduction, one of the objectives of the present study was to check whether the climate modes still dominate the interannual signal in coastal sea level globally, using the new network of altimetry-based virtual coastal stations located very close to the coast (at distances less than 8 km). Another objective was to investigate how far the interannual coastal sea level signal remains coherent when the distance from the coast increases towards the open ocean.

Our analysis at the virtual stations confirms the dominant influence of ENSO/MEI along the coasts of the eastern Pacific Ocean and Pacific side of southeast Asian coasts, as well as NAO on the Atlantic coasts, and IOD along North Indian Ocean coasts. The dominant EOF mode at the virtual coastal stations and the ones obtained from gridded sea level data in three successive bands (0-50 km, 50-100 km and 100-500 km from the coast) are similar, i.e., related to ENSO.

We have here focused on the influence of internal climate modes at the coast, with a global perspective. Further studies should be devoted to investigate the physical drivers of the coastal changes depending on regions, e.g., the effects of wind forcing and associated heat and water mass redistribution at the coast and offshore. It could be done using ocean reanalyses which we have shown give similar results than altimetry in terms of dominant EOF modes in the interannual variability of coastal sea level.

Our study has revealed two novel results: (1) a regime change in sea level between 2008 and 2012 with a strong sea level increase beyond that date in most coastal regions, except in a narrow area of the western tropical Pacific, and (2) the presence of a 6-year signal in a number of

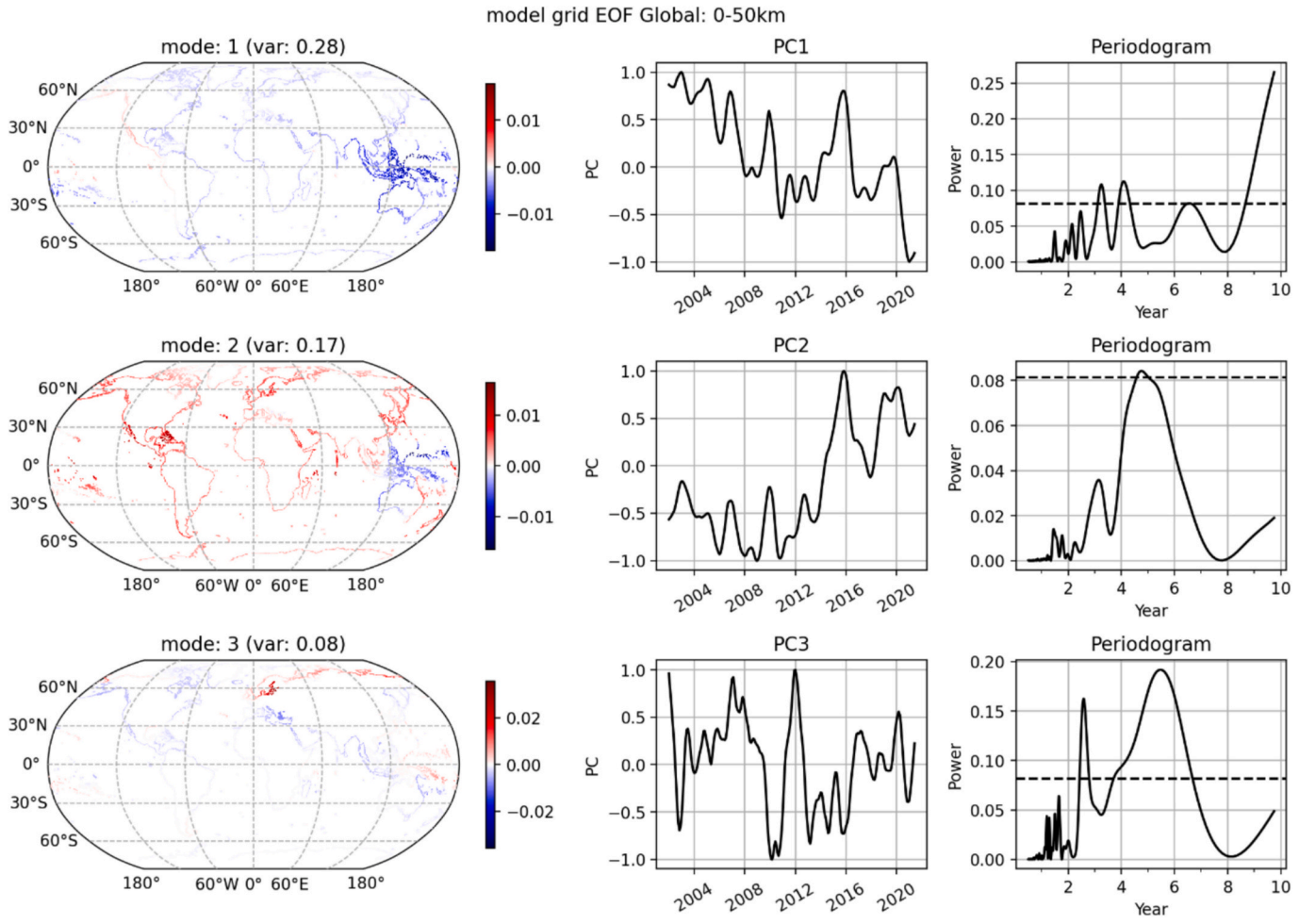

Fig. 6. First three modes of the EOF decomposition of global coastal sea level time series (deseasonalized but not detrended) over 2002–2021 (0-50 km from the coast) using data from the reanalyses ensemble mean. For each mode are shown the spatial distribution (left panel), the corresponding PC time series (middle panel) and the PC periodogram (right panel; the dashed line represents the 90 % confidence level). The PCs are normalized and the spatial maps are in meters.

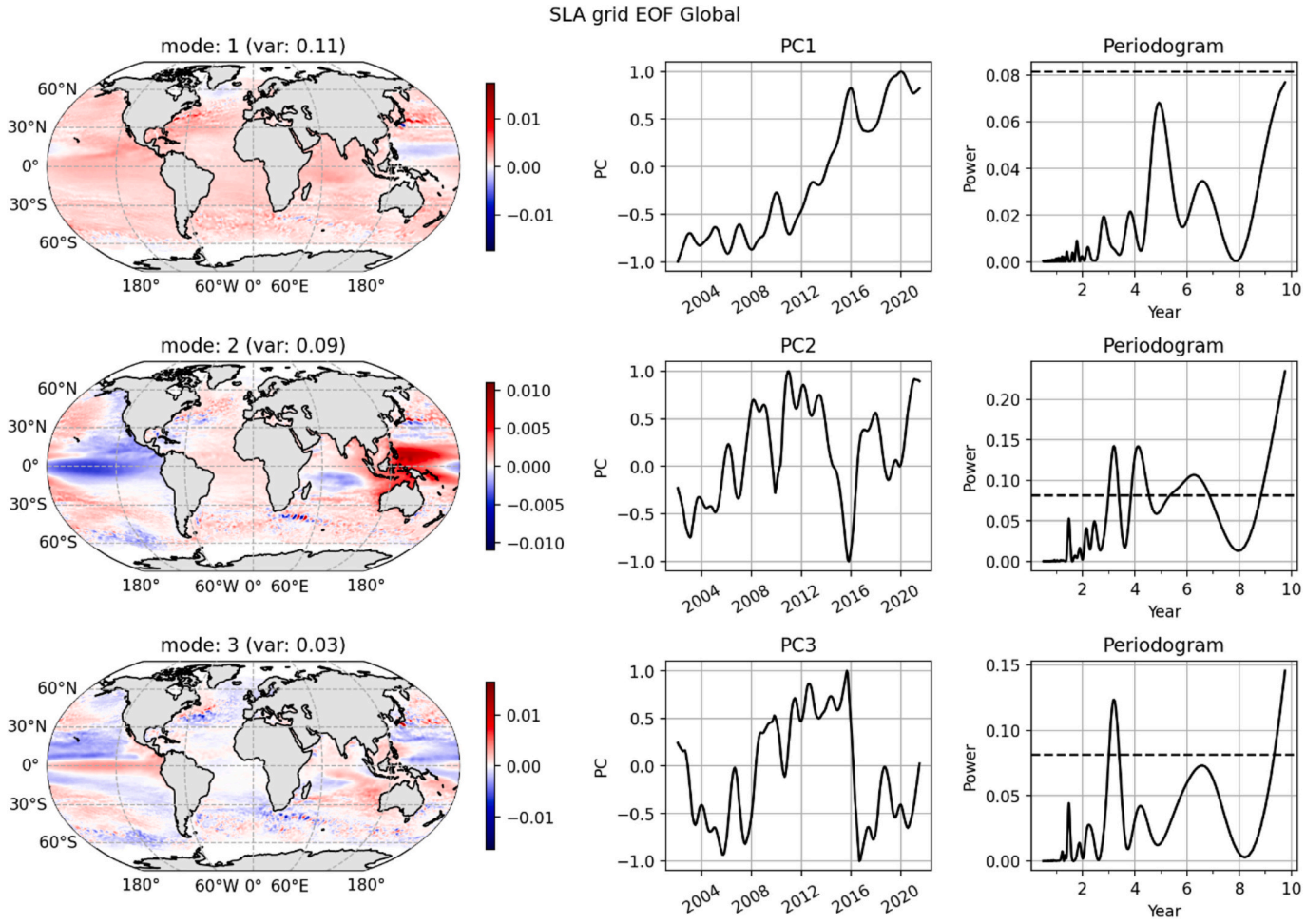

Fig. 7. First three modes of the EOF decomposition of the global C3S gridded altimetry data set (deseasonalized but not detrended). For each mode are shown the spatial distribution (left panel), the corresponding PC time series (middle panel) and the PC periodogram (right panel; the dashed line represents the 90 % confidence level). The PCs are normalized and the spatial maps are in meters.

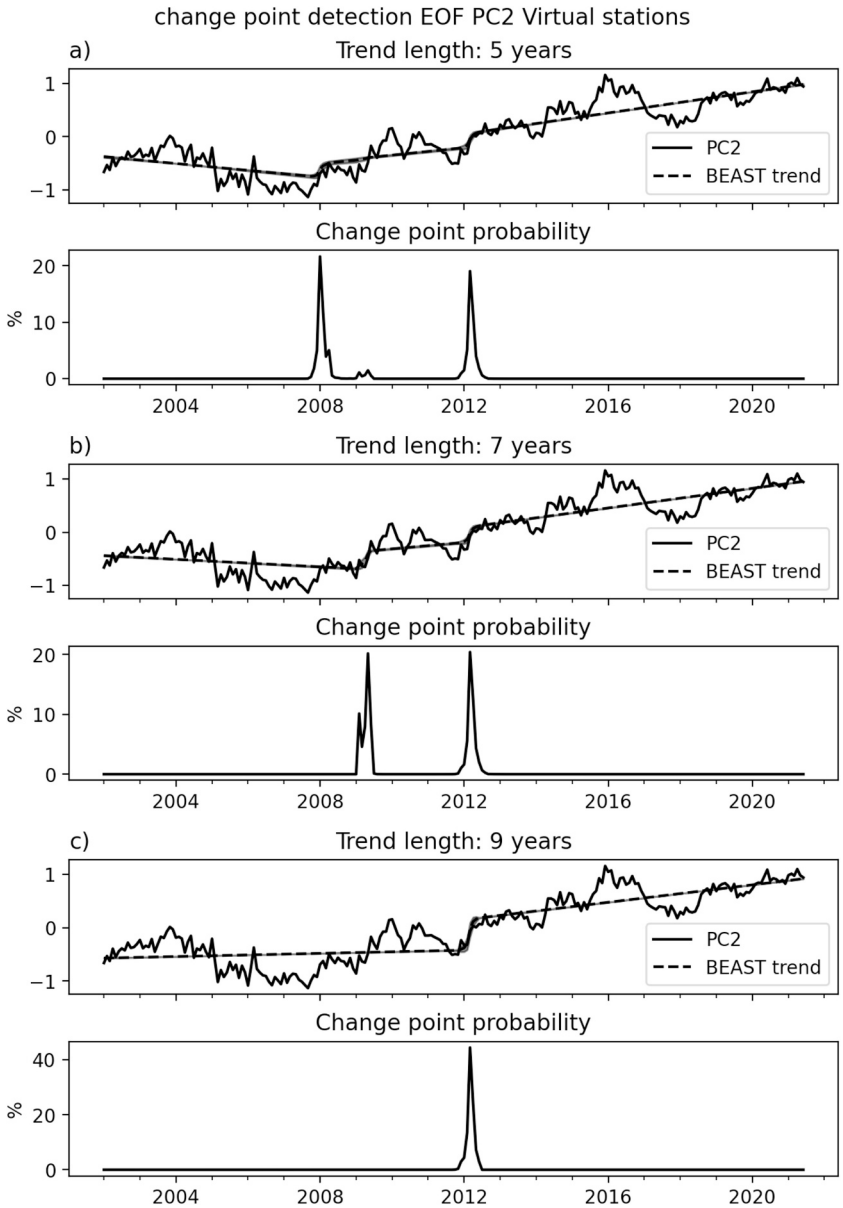

Fig. 8. Detection of a change in trend in the PC mode 2 of the EOF decomposition of the coastal sea level time series at the 1132 virtual stations, using the BEAST tool. (a) Trend length of 5 years. (b) Trend length of 7 years. (c) Trend length of 9 years. For each case, the upper panel shows original PC time series, and the lower panel shows the probability of trend change over the studied time period.

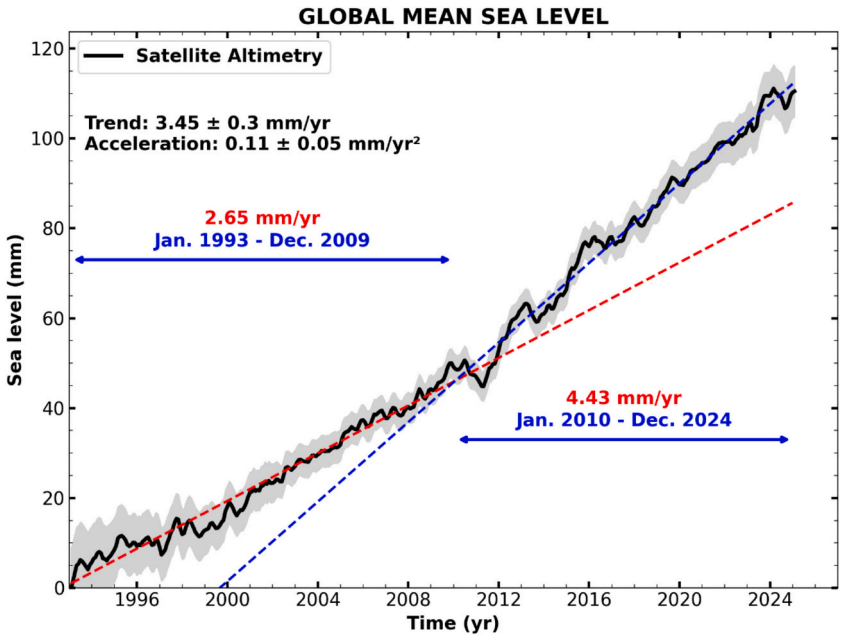

Fig. 9. Altimetry-based global mean sea level over January 1993–December 2024 (black curve). The dashed red and blue curves represent the GMSL slopes computed over 1993–2009 and 2010–2024. Data from AVISO (www.aviso.fr).

coastal regions, such as the Northeast Pacific north of 40°N, the Northeastern Indian Ocean and the Indian coast of Indonesia.

In several regions, the results presented here show evidence of a regime shift in coastal/near coastal sea level between 2008 and 2012. This is particularly visible along the coasts of Northwest and Northeast Atlantic, Caribbean and Gulf of Mexico, and African coasts. It is also seen in the open ocean and possibly in the GMSL. As briefly discussed in Section 6, such a regime shift may not be limited to sea level but may be a more global phenomenon possibly driven by decadal climate variability and a phase shift of the PDO, as well as an increase in radiative forcing on climate.

Concerning the 6-year cycle also highlighted in the EOF analysis, it is well seen at some virtual coastal stations, but somewhat less well resolved in the gridded data, although still present. This 6-year cycle has been recently discovered in several climate parameters as well as in the zonal wind circulation of the atmosphere. However, the link of the 6-year oscillation of the climate system with the 6-year cycle of the rotation of the solid Earth, magnetic field and motions of the fluid core is not yet elucidated. To remain within the context of the present study, its presence in coastal sea level may eventually result from along shore wind forcing. This could be the object of a future investigation.

Finally, the results presented here will eventually generate further investigations about the physical processes able to explain the different observations highlighted in the present study.

Credit authorship contribution statement

Lancelot Leclercq: Methodology, Visualization, Data curation, Validation, Formal analysis, Software. **Habib B. Dieng:** Writing – review & editing, Validation. **Anny Cazenave:** Supervision, Conceptualization, Writing – original draft, Methodology, Validation. **Florence Birol:** Writing – review & editing, Validation, Supervision. **Julius Oelsmann:** Validation, Supervision, Writing – review & editing. **Marcello Passaro:** Validation, Supervision, Writing – review & editing. **Svetlana Jevrejeva:** Supervision, Writing – review & editing, Validation. **Erwin Bergsma:** Writing – review & editing. **Sarah Connors:** Writing – review & editing.

Declaration of competing interest

The authors declare no conflict of interest relevant to this study.

The authors declare the following financial interests/personal relationships which may be considered as potential competing interests:

Lancelot Leclercq reports a relationship with European Space Agency that includes: funding grants. If there are other authors, they declare that they have no known competing financial interests or personal relationships that could have appeared to influence the work reported in this paper.

Acknowledgements

We thank two anonymous reviewers for their useful comments. This study was carried out in the context of the Climate Change Initiative (CCI) Coastal Sea Level project supported by the European Space Agency (https://climate.esa.int/en/projects/sea-level). L.L. is supported by this ESA CCI project (grant number 4000126561/19/I-NB).

Data availability

Data will be made available on request.

References

Abarca del Rio, R., Gambis, D., Salstein, D.A., 2000. Interannual signals in length of day and atmospheric angular momentum. Ann. Geophys. 18, 347–364. https://doi.org/10.1007/s00585-000-0347-9.

Amano, M., Tachibana, Y., Ando, Y., 2023. Consideration of whether a climatic regime shift has prevented the occurrence of a cold summer in Northeast Eurasia since 2010. J. Clim. 36, 8059–8071. https://doi.org/10.1175/JCLI-D-23-0191.1.

An, S.-I., Wang, C., 2020. In: Mechoso, C.R., Mechoso, C.R. (Eds.), Teleconnections in the Atmosphere, in Interacting Climates of Ocean Basins, Observations, Mechanisms, Predictability and Impacts. Cambridge University Press, pp. 54–88. https://doi.org/10.1017/9781108610995.

Bandara, K., Hyndman, R.J., Bergmeir, C., 2021. MSTL: a seasonal-trend decomposition algorithm for time series with multiple seasonal patterns. Int. J. Operat. Res. 1 (1), 1. https://doi.org/10.1504/IJOR.2022.10048281.

Benveniste, J., Birol, F., Calafat, F., Cazenave, A., Dieng, H., Gouzenes, Y., Legeais, J.F., Léger, F., Niño, F., Passaro, M., Schwatke, C., Shaw, A., 2020. Coastal Sea level anomalies and associated trends from Jason satellite altimetry over 2002–2018. Sci. Data 7, 357. https://doi.org/10.1038/s41597-020-00694-w.

Birol, F., Léger, F., Passaro, M., Cazenave, A., Niño, F., Calafat, F.M., Shaw, A., Legeais, J.-F., Gouzenes, Y., Schwatke, C., Benveniste, J., 2021. The X-TRACK/ALES

multi-mission processing system: New advances in altimetry towards the coast. Adv. Space Res. 67, 2398–2415. https://doi.org/10.1016/j.asr.2021.01.049.
Camargo, C.M.I., Piecuch, C.G., Raubenheimer, B., 2024. From shelfbreak to shoreline: Coastal Sea level and local ocean dynamics in the Northwest Atlantic. Geophys. Res. Lett. 51, e2024GL109583. https://doi.org/10.1029/2024GL109583.
Cazenave, A., Moreira, L., 2022. Contemporary Sea-level changes from global to local scales: a review. Proc. Roy. Soc. A 478, 20220049. https://doi.org/10.1098/rspa.2022.0049.
Cazenave, A., Gouzenes, Y., Birol, F., Leger, F., Passaro, M., Calafat, F.M., Shaw, A., Nino, F., Legeais, J.F., Oelsmann, J., Restano, M., Benveniste, J., 2022. Sea level along the world's coastlines can be measured by a network of virtual altimetry stations. Commun. Earth Environ. 3, 117. https://doi.org/10.1038/s43247-022-00448-z.
Cazenave, A., Pfeffer, J., Mandea, M., Dehant, V., 2023. ESD ideas: a 6-year oscillation in the whole Earth system? Earth Syst. Dyn. 14, 733–735. https://doi.org/10.5194/esd-14-733-2023.
Cazenave, A., Pfeffer, J., Mandea, M., Dehant, V., Gillet, N., 2025. Why is the Earth system oscillating at a 6-year period? Surv. Geophys. https://doi.org/10.1007/s10712-024-09874-4 in press.
Chang, P., Richter, I., Dijkstra, H., Wieners, C., Myers, T.A., 2020. In: Mechoso, C.R. (Ed.), Atmosphere-Ocean Interactions, in Interacting Climates of Ocean Basins, Observations, Mechanisms, Predictability and Impacts. Cambridge University Press, pp. 89–119. https://doi.org/10.1017/9781108610995.
Chao, B.F., Yu, Y., 2020. Variation of the equatorial moments of inertia associated with a 6-year westward rotary motion in the Earth. Earth Planet. Sci. Lett. 542, 116316. https://doi.org/10.1016/j.epsl.2020.116316.
Cheng, X., Zhao, M., Duan, W., Jiang, L., Chen, J., Yang, C., Zhou, Y., 2023. Regime shift of the sea level trend in the South China Sea modulated by the tropical Pacific decadal variability. Geophys. Res. Lett. 50, e2022GL102708. https://doi.org/10.1029/2022GL102708.
Cisse, C.O.T., Almar, R., Youm, J.P.M., Jolicoeur, S., Taveneau, A., Sy, B.A., Sakho, I., Sow, B.A., Dieng, H., 2022. Extreme coastal water levels evolution at Dakar (Senegal, West Africa). Climate 11 (1), 6. https://doi.org/10.3390/cli11010006.
Currie, R.G., 1973. Geomagnetic line spectra −2 to 70 years. Astrophys. Space Sci. 21, 425–438.
Dangendorf, S., Frederikse, T., Chafik, L., Klinck, J., Ezer, T., Hamlington, B., 2021. Data-driven reconstruction reveals large-scale ocean circulation control on coastal sea level. Nat. Clim. Chang. 11 (6), 514–520.
Dangendorf, S., Hendricks, N., Sun, Q., Klinck, J., Ezer, T., Frederikse, T., Calafat, F.M., Wahl, T., Törnqvist, T.E., 2023. Acceleration of U.S. Southeast and Gulf coast sea-level rise amplified by internal climate variability. Nat. Commun. 14, 1935. https://doi.org/10.1038/s41467-023-37649-9.
Dieng, H.B., Cazenave, A., Meyssignac, B., Ablain, M., 2017. New estimate of the current rate of sea level rise from a sea level budget approach. Geophys. Res. Lett. 44, 3744–3751. https://doi.org/10.1002/2017GL073308.
Dieng, H.B., Dadou, I., Léger, F., Morel, Y., Jouanno, J., Lyard, F., Allain, D., 2021. Sea level anomalies using altimetry, model and tide gauges along the African coasts in the Eastern Tropical Atlantic Ocean: inter-comparison and temporal variability. Adv. Space Res. 68, 534–552. https://doi.org/10.1016/j.asr.2019.10.019.
Dieng, H.B., et al., 2025. Coastal sea level change in west Africa. In preparation.
Dièye, A., Sow, B.A., Dieng, H.B., Marchesiello, P., Descroix, L., 2023. Impact of climate variability modes on trend and interannual variability of sea level near the West African coast. Afr. J. Environ. Sci. Technol. 17 (7), 157–166. https://doi.org/10.5897/AJEST2022.3173.
Fasullo, J.T., Gent, P.R., Nerem, R.S., 2020. Sea level rise in the CESM large ensemble: the role of individual climate forcings and consequences for the coming decades. J. Clim. 33, 6911–6927. https://doi.org/10.1175/JCLI-D-19-1001.1.
Frederikse, T., Riva, R., Kleinherenbrink, M., Wada, Y., den Broeke, M., Marzeion, B., 2016. Closing the sea level budget on a regional scale: Trends and variability on the Northwestern European continental shelf. Geophys. Res. Lett. 43, 10,864–10,872. https://doi.org/10.1002/2016GL070750.
Frederikse, T., Simon, K., Katsman, C.A., Riva, R., 2017. The sea-level budget along the Northwest Atlantic coast: GIA, mass changes, and large-scale ocean dynamics. J. Geophys. Res. Oceans 122, 5486–5501. https://doi.org/10.1002/2017JC012699.
Garric, G., Parent, L., 2017. Quality Information Document for Global 1330 Ocean Reanalysis Products Global-Reanalysis-Phy-001-025. Available online at: https://catalogue.marine.copernicus.eu/documents/QUID/CMEMS-GLO-QUID-001-025.pdf.
Ghomsi, F., et al., 2024. Sea level variability in Gulf of Guinea from satellite altimetry. Sci. Rep. 14, 1. https://doi.org/10.1038/s41598-024-55170-x.
Gillet, N., Jault, D., Canet, E., et al., 2010. Fast torsional waves and strong magnetic field within the Earth's core. Nature 465, 74–77. https://doi.org/10.1038/nature09010.
Gillet, N., Gerick, F., Jault, D., Schwaiger, T., Aubert, J., Istas, M., 2022. Satellite magnetic data reveal interannual waves in Earth's core. Proc. Natl. Acad. Sci. 119 (13), e2115258119. https://doi.org/10.1073/pnas.2115258119.
Guérou, A., Meyssignac, B., Prandi, P., Ablain, M., Ribes, A., Bignalet-Cazalet, F., 2023. Current observed global mean sea level rise and acceleration estimated from satellite altimetry and the associated measurement uncertainty. Ocean Sci. 19, 431–451. https://doi.org/10.5194/os-19-431-2023.
Hamlington, B.D., et al., 2020. Understanding of Contemporary Regional Sea-Level Change and the Implications for the Future. Rev. Geophys. 58, e2019RG000672. https://doi.org/10.1029/2019RG000672.
Hamlington, B.D., et al., 2024. The rate of global sea level rise doubled during the past three decades. Commun. Earth Environ. 5, 601. https://doi.org/10.1038/s43247-024-01761-5.
Han, W., Meehl, G., Stammer, D., Hu, A., Hamlington, B., Kenigson, J., et al., 2017. Spatial patterns of sea level variability associated with natural internal climate modes. Surv. Geophys. 38 (1), 217–250. https://doi.org/10.1007/s10712-016-9386-y.
Han, W., Stammer, D., Thompson, P., Ezer, T., Palanisamy, H., Zhang, X., Domingues, C. M., Zhang, L., Yuan, D., 2019. Impacts of basin-scale climate modes on coastal sea level: a review. Surv. Geophys. 40, 1493–1541. https://doi.org/10.1007/s10712-019-09562-8.
Hartmann, B., Wendler, G., 2005. The significance of the 1976 Pacific climate shift in the climatology of Alaska. J. Clim. 18, 4824–4839.
Hermans, T.H.J., Le Bars, D., Katsman, C.A., Camargo, C.M.L., Gerkema, T., Calafat, F. M., et al., 2020. Drivers of interannual sea level variability on the northwestern European shelf. J. Geophys. Res. Oceans 125, e2020JC016325. https://doi.org/10.1029/2020JC016325.
Hodnebrog, O., et al., 2024. Recent reductions in aerosol emissions have increased Earth's energy imbalance. Commun. Earth Environ. 5, 166.
IPCC, 2019. In: Pörtner, H.-O., Roberts, D.C., Masson-Delmotte, V., Zhai, P., Tignor, M., Poloczanska, E., Mintenbeck, K., Alegría, A., Nicolai, M., Okem, A., Petzold, J., Rama, B., Weyer, N.M. (Eds.), IPCC Special Report on the Ocean and Cryosphere in a Changing Climate. Cambridge University Press, Cambridge, UK and New York, NY, USA. https://doi.org/10.1017/9781009157964, 755 pp.
IPCC, 2022. In: Pörtner, H.-O., Roberts, D.C., Tignor, M., Poloczanska, E.S., Mintenbeck, K., Alegría, A., Craig, M., Langsdorf, S., Löschke, S., Möller, V., Okem, A., Rama, B. (Eds.), Climate Change 2022: Impacts, Adaptation and Vulnerability. Contribution of Working Group II to the Sixth Assessment Report of the Intergovernmental Panel on Climate Change. Cambridge University Press, Cambridge, UK and New York, NY, USA. https://doi.org/10.1017/9781009325844, 3056 pp.
Kucharski, F., Biastoch, A., Ashok, K., Yuan, D., 2020. In: Mechoso, C.R. (Ed.), Indian Ocean Variability and Interactions, in Interacting Climates of Ocean Basins, Observations, Mechanisms, Predictability and Impacts. Cambridge University Press, pp. 153–185. https://doi.org/10.1017/9781108610995.
Leclercq, L., Cazenave, A., Birol, F., et al., 2025. Coastal Sea level rise at altimetry-based virtual stations in the Gulf of Mexico. Adv. Space Res. 75, 1636–1652. https://doi.org/10.1016/j.asr.2024.11.069.
Little, C.M., Piecuch, C.G., Ponte, R.M., 2021. North American east coast sea level exhibits high power and spatiotemporal complexity on decadal timescales. Geophys. Res. Lett. 48, e2021GL093675. https://doi.org/10.1029/2021GL093675.
Lyu, K., Zhang, X., Church, J.A., Hu, J., Yu, J., 2017. Distinguishing the quasi-decadal and multidecadal sea level and climate variations in the Pacific: Implications for the ENSO-like low-frequency variability. J. Clim. 30 (13), 5097–5117. https://doi.org/10.1175/JCLI-D-17-0004.1.
MacLachlan, C., Arribas, A., Peterson, K.A., Maidens, A., Fereday, D., Scaife, A.A., Gordon, M., Vellinga, M., Williams, A., Comer, R.E., Camp, J., Xavier, P., 2015. Description of GloSea5: the Met Office high resolution seasonal forecast system. Q. J. R. Meteorol. Soc. https://doi.org/10.1002/qj.2396.
Mandea, M., Panet, I., Lesur, V., De Viron, O., Diament, M., Le Mouël, J.L., 2012. Recent changes of the Earth's core derived from satellite observations of magnetic and gravity fields. Proc. Natl. Acad. Sci. 109 (47), 19129–19133. https://doi.org/10.1073/pnas.1207346109.
Mandea, M., Narteau, C., Panet, I., Le Mouël, J.L., 2015. Gravimetric and magnetic anomalies produced by dissolution-crystallization at the core-mantle boundary. J. Geophys. Res. Solid Earth 120 (9), 5983–6000. https://doi.org/10.1002/2015JB012048.
Mechoso, C.R., 2020. Interacting climates of ocean basins, Observations, mechaisms, predictability and impacts, 341 pages. Cambridge University Press. https://doi.org/10.1017/9781108610995.
Merchant, C.J., Allan, R.P., Emberry, O., 2025. Quantifying the acceleration of multidecadal global sea surface warming friven by Earth's energy imbalance. Environ. Res. Lett. 20, 024037. https://doi.org/10.1088/1748-9326/adaa8a.
Miller, A., Cayan, D., Barnett, T., Graham, N., Oberhuber, J., 1994. The 1976–77 climate shift of the Pacific Ocean. Oceanography 7, 21–26.
Moreira, L., Cazenave, A., Palanisamy, H., 2021. Influence of interannual variability in estimating the rate and acceleration of present-day global mean sea level. Glob. Planet. Chang. 199, 103450. https://doi.org/10.1016/j.gloplacha.2021.103450.
Nerem, R.S., Beckley, B.D., Fasullo, J.T., Hamlington, B.D., Masters, D., Mitchum, G.T., 2018. Climate-change–driven accelerated sea-level rise detected in the altimeter era. Proc. Natl. Acad. Sci. 115, 2022–2025. https://doi.org/10.1073/pnas.1717312115.
Oelsmann, J., Calafat, F.M., Passaro, M., Hughes, C., Richter, K., Piecuch, C., et al., 2024. Coherent modes of global coastal sea level variability. J. Geophys. Res. Oceans 129, e2024JC021120. https://doi.org/10.1029/2024JC021120.
Palanisamy, H., Meyssignac, B., Cazenave, A., Delcroix, T., 2015. Is the anthropogenic sea level fingerprint already detectable in the Pacific Ocean? Environ. Res. Lett. 10, 124010. https://doi.org/10.1088/1748-9326/10/12/124010.
Papdopoulos, A., Tsimplis, M.N., 2006. Coherent coastal sea level variability at interdecadal and iterannual scales from tide gauges. J. Coast. Res. 22 (3), 625–639. https://www.jstor.org/stable/4300317.doi.org/.
Passaro, M., Cipollini, P., Vignudelli, S., Quartly, G.D., Snaith, H.M., 2014. ALES: a multi-mission adaptive subwaveform retracker for coastal and open ocean altimetry. Remote Sens. Environ. 145, 173–189. https://doi.org/10.1016/j.rse.2014.02.008.
Passaro, M., Nadzir, Z.A., Quartly, G.D., 2018. Improving the precision of sea level data from satellite altimetry with high-frequency and regional sea state bias corrections. Remote Sens. Environ. 218, 245–254. https://doi.org/10.1016/j.rse.2018.09.007.
Pfeffer, J., Cazenave, A., Rosat, S., Moreira, L., Mandea, M., Dehant, V., 2023. A 6-year cycle in the earth system. Glob. Planet. Chang. 229, 104245. https://doi.org/10.1016/j.gloplacha.2023.104245.
Piecuch, C.G., Bittermann, K., Kemp, A.C., Ponte, R.M., Little, C.M., Engelhart, S.E., Lentz, S.J., 2018. River-discharge effects on United States Atlantic and Gulf coast

sea-level changes. Proc. Natl. Acad. Sci. 115, 7729–7734. https://doi.org/10.1073/pnas.1805428115.
Power, S., Lengaigne, M., Capotondi, A., Khodri, M., Vialard, J., Jebri, B., et al., 2021. Decadal climate variability in the tropical Pacific: characteristics, causes, predictability, and prospects. Science 374 (6563), eaay9165. https://doi.org/10.1126/science.aay9165.
Preisendorfer, R.W., 1988. In: Mobley, C.D. (Ed.), Principal Component Analysis in Meteorology and Oceanography, vol. 425. Elsevier Science, New York.
Qu, Y., Jevrejeva, S., Wang, S., 2023. Unraveling Regional patterns of Sea Level Acceleration over the China Seas. Remote Sens. 15, 4448. https://doi.org/10.3390/rs15184448.
Rodriguez-Fonseca, B., et al., 2020. In: Mechoso, C.R. (Ed.), Interacting Interannual Variability of the Pacific and Atlantic Oceans, in Interacting Climates of Ocean Basins, Observations, Mechanisms, Predictability and Impacts. Cambridge University Press, pp. 120–152. https://doi.org/10.1017/9781108610995.
Royston, S., Bingham, R.J., Bamber, J.I., 2022. Attributing decadal climate variability in coastal sea level trends. Ocean Sci. 18, 1093–1107. https://doi.org/10.5194/os-18-1093-2022.
Stammer, D., Cazenave, A., Ponte, R.M., Tamisiea, M.E., 2013. Causes for contemporary regional sea level changes. Annu. Rev. Mar. Sci. 5, 21–46. https://doi.org/10.1146/annurev-marine-121211-172406.
Steinberg, J.M., Piecuch, C.G., Hamlington, B.D., Thompson, P.R., Coats, S., 2024. Influence of deep-ocean warming on coastal sea-level decadal trends in the Gulf of Mexico. J. Geophys. Res. Oceans 129, e2023JC019681. https://doi.org/10.1029/2023JC019681.
Storto, A., Masina, S., 2016. C-GLORSv5: an improved multipurpose global ocean eddy-permitting physical reanalysis. Earth Syst. Sci. Data 8, 679–696. https://doi.org/10.5194/essd-8-679-2016.
Thompson, B., Jevrejeva, S., Zachariah, J., Faller, D.G., Tkalich, P., 2023. Impact of mass redistribution on regional sea level changes over the South China Sea shelves. Geophys. Res. Lett. 50, e2023GL105740. https://doi.org/10.1029/2023GL105740.
VanderPlas, J.T., 2018. Understanding the Lomb–Scargle Periodogram. Astrophys. J. 236 (16). https://doi.org/10.3847/1538-4365/aab766.
Wang, L., Lyu, K., Zhuang, W., Zhang, W., Makarim, S., Yan, X., 2021. Recent shift in the warming of the southern oceans modulated by decadal climate variability. Geophys. Res. Lett. 48 (3), e2020GL090889. https://doi.org/10.1029/2020GL090889.
Wang, O., Lee, T., Piecuch, C.G., Fukumori, I., Fenty, I., Frederikse, T., et al., 2022. Local and remote forcing of interannual sea-level variability at Nantucket Island. J. Geophys. Res. Oceans 127, e2021JC018275. https://doi.org/10.1029/2021JC018275.
Watkins, M., Fu, Y., Gross, R., 2018. Earth's subdecadal angular momentum balance from deformation and rotation Data. Sci. Rep. 8, 13761. https://doi.org/10.1038/s41598-018-32043-82017.
Wise, A., Calafat, F.M., Hughes, C.W., Jevrejeva, S., Katsman, C.A., Oelsmann, J., et al., 2024. Using shelf-edge transport composition and sensitivity experiments to understand processes driving sea level on the Northwest European shelf. J. Geophys. Res. Oceans 129, e2023JC020587. https://doi.org/10.1029/2023JC020587.
Woodworth, P.L., Melet, A., Marcos, M., Ray, R.D., Wöppelmann, G., Sasaki, Y.N., Cirano, M., Hibbert, A., Huthnance, J.M., Monserrat, S., Merrifield, M.A., 2019. Forcing factors affecting sea level changes at the coast. Surv. Geophys. 40, 1351–1397. https://doi.org/10.1007/s10712-019-09531-1.
Woppelmann, G., Marcos, M., 2016. Considering vertical land motion in understanding sea level change and variability. Rev. Geophys. 54. https://doi.org/10.1002/2015RG000502.
Wu, L., Lee, D.E., Liu, Z., 2005. The 1976/1977 North Pacific climate regime shift: the role of subtropical ocean adjustment and coupled ocean-atmosphere feedbacks. J. Clim. 18, 5125–5140.
Yin, J., 2023. Rapid decadal acceleration of sea level rise along the U.S. East and Gulf Coasts during 2010–22 and its impact on Hurricane-Induced storm surge. J. Clim. 36, 4511–4529. https://doi.org/10.1175/JCLI-D-22-0670.1.
Yu, J.-Y., et al., 2020. Variability of the oceans. In: Mechoso, C.R. (Ed.), Interacting Climates of Ocean Basins, Observations, Mechanisms, Predictability and Impacts. Cambridge University Press, pp. 1–53. https://doi.org/10.1017/9781108610995.
Zhao, K., et al., 2019. Detecting change point, trend and seasonality in satellite time series data to track abrupt changes and non linear dynamics: a Bayesian ensemble algorithm. Remote Sens. Environ. 232, 111181.
Zuo, H., Balmaseda, M.A., Tietsche, S., Mogensen, K., Mayer, M., 2019. The ECMWF operational ensemble reanalysis–analysis system for ocean and sea ice: a description of the system and assessment. Ocean Sci. 15, 779–808.
Zwally, H.J., Robbins, J.W., Luthcke, S.B., Loomis, B.D., Rémy, F., 2021. Mass balance of the Antarctic ice sheet 1992–2016: reconciling results from GRACE gravimetry with ICESat, ERS1/2 and Envisat altimetry. J. Glaciol. 67, 533–559. https://doi.org/10.1017/jog.2021.8.